**Kingdom of Saudi Arabia**
**Imam Mohammad bin Saud Islamic**
**University College of Science**
**Chemistry Department**

# Preparation of $AlMgO_4$, 2.5%$MoO_3$@$AlMgO_4$, 5%$MoO_3$@$AlMgO_4$, and 10 %$MoO_3$@$AlMgO_4$ composites for removing Ciprofloxacin and oxytetracycline from contaminated water.

*Research submitted as partial fulfillment of the requirements for the completion of the BSc Degree in Chemistry*

**By**
**Meshal Mohammad Hameed Alrasheedi (439025161)**
**&**
**Mohammed abdulmohsen Mohammed almass (439025829)**
**&**
**Salman Ahmed Abdullah Al Ghamdi (441015116)**
**&**
**Mishari bin Saad bin Embarak Al-Zahrani (439014991)**

## Supervisor

**Dr. Babiker Y. Abdulkhair**

**Fabruray - 2024**

## *Acknowledgement & Dedication*

***Our heartfelt gratitude goes to our supervisor, Dr. Babiker, for all of his help and guidance.***

***Please accept our heartfelt gratitude for the chemistry faculty's hard work.***

***This endeavor is in honor of our loved ones, who have always supported us and inspired us to keep going.***

| No. | Contents | Page No. |
|---|---|---|
| | Abstract (English) | 6 |
| | Abstract (Arabic) | 7 |
| | Chapter 1<br>Introduction and literature review | |
| 1. | Introduction | 8 |
| 1.1 | Preparation of nanomaterials | 8 |
| 1.2 | Water pollution | 9 |
| 1.3. | Aim of the study | 14 |
| | Chapter 2<br>Materials and methods | |
| 2.1 | Materials | 16 |
| 2.2. | Preparation of $MgAl_2O_4$ and its $MoO_3$ composites | 16 |
| 2.3. | Preparation of CIP and OXY solutions | 16 |
| 2.4. | Adsorption of CIP and OXY | 17 |
| | Chapter 3<br>Results and discussion | |
| 3. | Results and discussion | 19 |
| 3.1 | Contact time study | 19 |
| 3.2 | Adsorption rate order | 24 |
| 3.3 | Adsorption control mechanism | 34 |
| 3.4. | Conclusion | 45 |
| 46 | Reference | 46 |

| Figures | | |
|---|---|---|
| **Fig. No.** | **Caption** | **Page No.** |
| **1** | **The contact time trend of CIP sorption onto the $MgAl_2O_4$ nanocomposite.** | **20** |
| **2** | **The contact time trend of CIP sorption onto the 2.5%$MoO_3$@$MgAl_2O_4$ nanocomposite.** | **20** |
| **3** | **The contact time trend of CIP sorption onto the 5%$MoO_3$@$MgAl_2O_4$ nanocomposite.** | **21** |
| **4** | **The contact time trend of CIP sorption onto the 10%$MoO_3$@$MgAl_2O_4$ nanocomposite.** | **21** |
| **5** | **The contact time trend of OXY sorption onto the $MgAl_2O_4$ nanocomposite.** | **22** |
| **6** | **The contact time trend of OXY sorption onto the 2.5%$MoO_3$@$MgAl_2O_4$ nanocomposite.** | **22** |
| **7** | **The contact time trend of OXY sorption onto the 5%$MoO_3$@$MgAl_2O_4$ nanocomposite.** | **23** |
| **8** | **The contact time trend of OXY sorption onto the 10%$MoO_3$@$MgAl_2O_4$ nanocomposite.** | **23** |
| **9** | **The PF investigation of CIP sorption onto $MgAl_2O_4$ composite.** | **25** |
| **10** | **The PF investigation of CIP sorption onto 2.5%$MoO_3$@$MgAl_2O_4$ composite.** | **25** |
| **11** | **The PF investigation of CIP sorption onto 5%$MoO_3$@$MgAl_2O_4$ composite.** | **26** |
| **12** | **The PF investigation of CIP sorption onto 10%$MoO_3$@$MgAl_2O_4$ composite.** | **26** |
| **13** | **The PF investigation of OXY sorption onto $MgAl_2O_4$ composite.** | **27** |
| **14** | **The PF investigation of OXY sorption onto 2.5%$MoO_3$@$MgAl_2O_4$ composite.** | **27** |
| **15** | **The PF investigation of OXY sorption onto 5%$MoO_3$@$MgAl_2O_4$ composite.** | **28** |
| **16** | **The PF investigation of OXY sorption onto 10%$MoO_3$@$MgAl_2O_4$ composite.** | **28** |
| **17** | **The PS investigation of CIP sorption onto $MgAl_2O_4$ composite.** | **29** |
| **18** | **The PS investigation of CIP sorption onto 2.5%$MoO_3$@$MgAl_2O_4$ composite.** | **29** |

| | | |
|---|---|---|
| 19 | The PS investigation of CIP sorption onto 5%$MoO_3$@$MgAl_2O_4$ composite. | 30 |
| 20 | The PS investigation of CIP sorption onto 10%$MoO_3$@$MgAl_2O_4$ composite. | 30 |
| 21 | The PS investigation of OXY sorption onto $MgAl_2O_4$ composite. | 31 |
| 22 | The PS investigation of OXY sorption onto 2.5%$MoO_3$@$MgAl_2O_4$ composite. | 31 |
| 23 | The PS investigation of OXY sorption onto 5%$MoO_3$@$MgAl_2O_4$ composite. | 32 |
| 24 | The PS investigation of OXY sorption onto 10%$MoO_3$@$MgAl_2O_4$ composite. | 32 |
| 25 | The LFD investigation of CIP sorption onto $MgAl_2O_4$ composite. | 35 |
| 26 | The LFD investigation of CIP sorption onto 2.5%$MoO_3$@$MgAl_2O_4$ composite. | 36 |
| 27 | The LFD investigation of CIP sorption onto 5%$MoO_3$@$MgAl_2O_4$ composite. | 36 |
| 28 | The LFD investigation of CIP sorption onto 10%$MoO_3$@$MgAl_2O_4$ composite. | 37 |
| 29 | The LFD investigation of OXY sorption onto $MgAl_2O_4$ composite. | 37 |
| 30 | The LFD investigation of OXY sorption onto 2.5%$MoO_3$@$MgAl_2O_4$ composite. | 38 |
| 31 | The LFD investigation of OXY sorption onto 5%$MoO_3$@$MgAl_2O_4$ composite. | 38 |
| 32 | The LFD investigation of OXY sorption onto 10%$MoO_3$@$MgAl_2O_4$ composite. | 39 |
| 33 | The LFD investigation of CIP sorption onto $MgAl_2O_4$ composite. | 39 |
| 34 | The LFD investigation of CIP sorption onto 2.5%$MoO_3$@$MgAl_2O_4$ composite. | 40 |
| 35 | The LFD investigation of CIP sorption onto 5%$MoO_3$@$MgAl_2O_4$ composite. | 40 |
| 36 | The LFD investigation of CIP sorption onto 10%$MoO_3$@$MgAl_2O_4$ composite. | 41 |
| 37 | The LFD investigation of OXY sorption onto $MgAl_2O_4$ composite. | 41 |
| 38 | The LFD investigation of OXY sorption onto 2.5%$MoO_3$@$MgAl_2O_4$ composite. | 42 |
| 39 | The LFD investigation of OXY sorption onto 5%$MoO_3$@$MgAl_2O_4$ composite. | 42 |
| 40 | The LFD investigation of OXY sorption onto 10%$MoO_3$@$MgAl_2O_4$ composite. | 43 |

**Abstract**

This work generated $MgAl_2O_4$, 2.5%$MoO_3$@ $MgAl_2O_4$, 5%$MoO_3$@ $MgAl_2O_4$, and 10%$MoO_3$@$MgAl_2O_4$ composites using a one-put quick approach. The produced composites were investigated for removing CIP and OXY from water. The $MgAl_2O_4$, 2.5%$MoO_3$@ $MgAl_2O_4$, 5%$MoO_3$@ $MgAl_2O_4$, and 10%$MoO_3$@$MgAl_2O_4$ showed CIP $q_t$ values of 137.0, 169.2, 190.9, and 156.0 mg $g^{-1}$, respectively, and OXY $q_t$ values of 121.4, 128.3, 153.9, and 128.4 mg $g^{-1}$ CIP sorption equilibrium took 60 minutes, while OXY sorption on the four sorbents took 30 minutes, and 90% of the uptake was accomplished during the first 20 and 10 minutes for CIP and OXY, respectively. PF and PS kinetic models were employed to investigate the CIP and OXY sorption rate order, while the IPD and LFD models were utilized to examine the rate-control-sorption step. The rate-order outputs of CIP removal showed that all sorbents suited PS except for 10%$MoO_3$@$MgAl_2O_4$, which followed PF. The OXY rate analysis showed that the four sorbents matched the PS except for 2.5% $MoO_3$@$MgAl_2O_4$, which fit the PF. CIP and OXY elimination by $MgAl_2O_4$, 2.5%$MoO_3$@ $MgAl_2O_4$, 5%$MoO_3$@ $MgAl_2O_4$, and 10%$MoO_3$@$MgAl_2O_4$ revealed to be controlled by the LFD.

## الملخص باللغة العربية

أنتج هذا العمل مركبات $MgAl_2O_4$, $2.5\%MoO_3@MgAl_2O_4$, $5\%MoO_3@MgAl_2O_4$ $10\%MoO_3@MgAl_2O_4$باستخدام طريقة سريعة من خطوة واحدة. تمت دراسة مقدرة المركبات المحضرة لإزالة CIP و OXY من الماء. أظهر$MgAl_2O_4$ ، $2.5\%MoO_3@MgAl_2O_4$، $5\%MoO_3@MgAl_2O_4$، و $10\%MoO_3@MgAl_2O_4$ قيم سعة امتزازمع CIP 137.0، 169.2، 190.9، و156.0 مجم/جرام، على التوالي، وقيم سعة الامتزازمع OXY تبلغ 121.4، 128.3، 153.9 و128.4 ملغم /جم على التوالي. استغرق توازن امتصاص 60 دقيقة مع CIP، بينما استغرق مع OXY 30 دقيقة على المواد المازة الأربعة ، وتم إنجاز 90% من الامتزاز خلال أول 20 و10 دقيقة لـ CIP وOXY، على التوالي. تم استخدام النماذج الحركية PF و PS لدراسة معدل الامتزاز CIP وOXY، بينما تم استخدام نماذج IPD و LFD لدراسة ميكانيكية الامتزاز. أظهرت مخرجات ترتيب معدل إزالة CIP أن جميع المواد المازة توافقت مع PS باستثناء $10\%MoO_3@MgAl_2O_4$ الذي يتبع PF. اما بالنسبة لـ OXY فان امتزازه على المواد الماصة الأربعة وافقت PS باستثناء 2.5%MoO@MgAl2O4 والتي وافقت PF. تم الكشف عن ميكانيكية إزالة CIP و OXY على $MgAl_2O_4$ ، و$2.5\%MoO_3@MgAl_2O_4$ ، $5\%MoO_3@MgAl_2O_4$، و $10\%MoO_3@MgAl_2O_4$ يتم التحكم فيها بواسطة LFD.

# *Chapter One*

## *Introduction and Literature Review*

# 1. Introduction

## 1.1. Preparation of nanomaterials

In recent years, scientists from several fields have extensively utilized nanoscale particles. However, there has been a recent resurgence in interest due to the ability to change these materials and make them more readily available [1]. Nanoscale materials find applications in many sectors, such as electronics, magnetism, biology, medicines, cosmetics, environmental science, catalysis, and materials science. The global surge in investment in nanotechnology research and development has been ascribed to the immense promise of this technology. Substantial expansion has been noted in nanotechnology research and financial support since 1999. The researchers aim to prioritize greater societal advancement and promote sustainable development. Efficient approaches may be developed to minimize the presence of contaminants and decrease their emissions by comprehending the processes of nanoparticle production and development, such as those occurring in combustion systems [2]. Many nanomaterial synthesis methods are bottom-up methods that combine atoms and molecules into nanoscale molecules. The second perspective is top-down, reducing bulk materials to nanoscale [3-5]; the methods for preparing nanomaterials include.

### 1.1.1. Solvothermal method

One of the most environmentally friendly and promising synthesis methods, the solvothermal (hydrothermal) approach, uses aqueous or nonaqueous solvents to

optimize particle size distribution and shape control. This technique homogenizes metal salts and adjusts the medium pH to alkaline with a basic solution. The target nanomaterial controls the homogenized solution's thermal treatment temperature and time. Time, temperature, medium, and precursors affect nanoparticle size and shape [6].

### 1.1.2. De-emulsification

Using a salting-out reagent and colloidal stabilizer, an aqueous gel dissolved the polymer and medication to create an emulsion. This method is suitable for thermally unstable materials since it does not require a temperature increase. Salting-out agents included magnesium, calcium, sodium sulfate, and sodium chloride. We also employed sucrose and other non-electrolytes. Some situations require a colloidal stabilizer like hydroxyethyl cellulose or polyvinylpyrrolidone. Diluting the organic solvent-water emulsion with extra water increases nanomaterial production. Wash the product to remove the stabilizer and salting agent [7].

### 1.1.3. Sol-gel method

A popular nanomaterials approach is the sol-gel procedure. A surfactant or nonaqueous solvent controls particle size in a suitable solvent during precursor reaction. In a liquid media, the particles prevented tiny crystals from clumping. Several famous chemists studied the periodic precipitation events that caused Liesegang rings and gel crystal formation [4, 8, 9]. This phenomenon has spurred much descriptive research. Roy and colleagues took advantage of

chemical homogeneity in colloidal gels. They improved them, allowing the sol-gel method to synthesize numerous ceramic oxide compositions containing Al, Si, Ti, Zr, etc. previously unreachable using ceramic powder methods. [10, 11]. The starting water and ammonia content, precursor, solvent, and reactant temperature determine the final spherical particle size. [12, 13].

### 1.1.4. Green synthesis

In green nanomaterial manufacturing, capping substrates might be plant extracts or microorganisms. Plant-based nanoparticles are mass-produced for biosynthesizing. Plants produce metallic nanoparticles from seeds, leaves, stems, roots, and latex. The safest technique to make nanoparticles was eco-friendly. The need for green metallic nanoparticle production has grown. We want to eliminate synthetic waste, chemical byproducts, and derivative substrates. Biomaterials from nature are useful for eco-friendly nanoparticle manufacturing. Scientists use bacteria, algae, fungi, and plants to make cheap, energy-efficient, and environmentally friendly metal nanoparticles. Green synthetic methods are replacing physicochemical ones in the industry [14, 15].

## 1.2. Water pollution

Water is crucial to human survival since water quality decline affects all life. Organic pollutants in water systems globally are a problem. Due to their widespread use and market demand, pharmaceuticals and chemical dyes are frequently used in water and sewage systems [16, 17]. The quality of drinking water has harmed public health. Water contamination causes most waterborne

illnesses, decimating urban populations. Due to this, people must drink untreated irrigation water, which has serious health consequences [16]. Understanding water pollutants' sources, interactions, and effects is essential to reducing their environmental impact and preserving ecosystems. The inappropriate disposal of aging pollutants, decontaminating equipment, and eradicating poorly manufactured and contaminated human and animal waste commodities might introduce such pollutants into water systems [17-19]. Dangerous aquatic pollution makes industrialized nations' water supply systems vulnerable. The US has more water than its rivers and lakes generate. Chemically hazardous groundwater may exist in some areas. Water pollutants include heavy metals, chlorinated hydrocarbons, organic pigments, industrial metal plating, and bacteria. Since World War II, synthetic chemical production and use have increased. The presence of these pollutants has contaminated water supplies. Examples include pesticide use, agricultural runoff, and improper industrial rubbish disposal into waterways. Incorrect chemical waste disposal in landfills, storage lagoons, treatment ponds, and other facilities can contaminate groundwater. Pollution and unequal distribution limit the usability of many global water sources, which appear infinite. Water scarcity affects many people worldwide, causing many wars. Groundwater, obtained by drilling, excavation, or springs, greatly influences river baseflow. Nearly 80% of ocean contaminants come from land-based sources, usually industrial operations or indirect dumping of human waste [20-22].

## 1.2. Water contamination

The Netherlands monitored the entire nation from 2010 to 2014. The operation detected high pesticide levels in groundwater wells, which is alarming. This study tested shallow groundwater samples from the Netherlands and Flanders for 405 compounds and 52 metabolites. The results showed neonicotinoids, which are mobile and persistent, at 0.12–0.01 g/L [23]. The Yangtze River Basin in Hubei Province, Central China, had high organochlorine and organophosphate pesticide levels. Sixteen groundwater samples from the given area contained fifteen organochlorines and four organophosphates. The four organophosphate pesticides' mean values were 196.01 ng/L for aldrin, dieldrin, and hexachlorocyclohexane. The water supply did not meet EPA criteria [24]. The phreatic aquifer beneath the Pampean area of Argentina contains organochlorine pesticides, indicating their long-term existence. Certain areas have high groundwater fluoride levels, according to multiple research. Avoid using groundwater with high fluoride contents for long durations. The health benefits of fluoride justify fluoridating public water sources. However, excessive fluoride absorption can cause dental and skeletal fluorosis. This study found that neonates and toddlers are more sensitive to dental fluorosis, a noncarcinogenic risk. A recent groundwater fluoride investigation in Agra City, India, found a wide range of amounts over the WHO 1.5 mg/L standard. The average fluoride concentration in 51 groundwater samples from Siddipet Vagu, India, was 3.7 ppm. 51% of samples exceeded the WHO safety standard of 1.5

mg/L for fluoride [25]. The study examined fifty borehole samples from intensive agriculture areas on the West Bank of the Nile River in Luxor Governorate, Egypt, and found that 62% were moderately vulnerable to groundwater pollution and 38% were high. Nitrate pollution from nitrogen-based fertilizers has poisoned 52% of the land. Recent research found that Chungcheong Province, South Korea, had a mean nitrate concentration of 12.4 mg/L [26]. Groundwater, oceans, and rivers contain pharmaceutical pollutants (PhCs) worldwide. Explaining humanity's dire situation may help: 50% of Earth's water has been poisoned since 1970. The US acknowledged PhC-polluted water as a public health risk in 1999 [27-30]. Over half of China's population drank polluted water during the same period. Indian rivers, groundwater, and water treatment facilities contain PhCs. These substances can reach 31.0 mg $L^{-1}$ [31, 32]. The need for infectious disease treatments and growing agricultural, poultry, and cattle output drive PhC pollution . The most representative tetracyclines include tigecycline, chlortetracycline, oxytetracycline (OXTC), and doxycycline [33]. Antibiotics and food preservatives have increased tetracycline (TC) use. Multiple studies have found TCs in soil and water reservoirs in the US, UK, and China [34]. The growth of PhCs in seas, oceans, rivers, and drinking water sources demonstrates that current treatment approaches are ineffective [35-43]. Thus, PhC prevention requires new methods. Nanomaterials have advanced the adsorption process,

which removes non-degradable water contaminants like heavy metals. This procedure is simple, energy-efficient, and does not release harmful fragments

### 1.3. Aim of the study

This study aimed to prepare $MgAl_2O_4$, 2.5%$MoO_3$@$MgAl_2O_4$, 5%$MoO_3$@$MgAl_2O_4$, and 10%$MoO_3$@$MgAl_2O_4$ triple composite as environmentally safe sorbents. A one-put route was adopted inorder to simplify the process. The study create prepared double and triple composites will tested for removing pharmaceutical pollutants exampled by oxytetracycline (OXY) and Ciprofloxacin (CIP), and their sorption kinetics would be investigated.

# *Chapter Two*

## *Materials and Methods*

## 2. Materials and methods

### 2.1 Materials

Ciprofloxacine (CIP) was provided from Rhanboxy, Mumbai, India. Oxytetracycline (OXY) and Ammonium Molybdate ($(NH_4)_2MoO_4$) were provided by Fluka, USA. Magnesium chloride-6-hydrate 99% ($MgCl_2$-$6H_2O$) and D(+)-Glucose monohydrate (GL) were provided from Riedel-de-Haen, Germany. Aluminum chloride hexahydrate 97% ($AlCl_3$-$6H_2O$) was purchased from (LOBA CHEMIE, Mumbai, India).

### 2.2. Preparation of $MgAl_2O_4$ and its $MoO_3$ composites

11.46 g of $AlCl_3$-$6H_2O$, 24.6 g of $MgCl_2$-$6H_2O$, and 10 g of GL were transferred to a 500 mL beaker. About 15 mL of distilled water was added. The mixture was turned into a clear solution by heating on a hotplate (120°C), then the hotplate temperature was raised (250°C) until the GL was carbonized. The obtained powder was grinned, transferred to a porcelain dish, and calcined at 600°C for 3.0 h. The process was repeated using the typical Al-Mg amounts with the addition of a proper amount of $(NH_4)_2MoO_4$ to obtain 2.5%$MoO_3$@$MgAl_2O_4$, 5%$MoO_3$@$MgAl_2O_4$, and 10%$MoO_3$@$MgAl_2O_4$.

### 2.3. Preparation of CIP and OXY solutions

0.1g of CIP was weighed using an analytical balance and transferred to a 1L volumetric flask to obtain 100 mg $L^{-1}$ CIP solution. Then, 600 mL of DW was added to the flask and put into an ultrasonic path. The resulting solution was

completed to the neck mark by DW. The 100 mg $L^{-1}$ OXY solution was prepared similarly to CIP.

**2.4. Adsorption**

0.05g of each sorbent ($MgAl_2O_4$, 2.5%$MoO_3$@$MgAl_2O_4$, 5%$MoO_3$@$MgAl_2O_4$, and 10%$MoO_3$@$MgAl_2O_4$) was measured in a separate 150 mL beaker. 100 mL of the 100 mg $L^{-1}$ CIP solution was poured into each beaker. A portion of the mixture was withdrawn till the CIP sorption reached the equilibrium. The aliquots were filtered via a 0.22μm syringe filter, and the absorbance was measured utilizing a UV-Vis-spectrophotometer ($\lambda_{max}$ = 270 nm). Also, the OXY adsorption ($\lambda_{max}$ = 275 nm) was studied similarly to CIP.

# *Chapter Three*

## *Results and Discussion*

## 3. Results and discussion

### 3.1. Contact time study

The contact time study of CIP and OXY sorption onto the as-prepared $MgAl_2O_4$, 2.5%$MoO_3$@$MgAl_2O_4$, 5%$MoO_3$@$MgAl_2O_4$, and 10%$MoO_3$@$MgAl_2O_4$ were studied. The CIP and OXY absorbance measured during the study were employed for calculating their remaining concentrations (unadsorbed) at each time interval via Eq. 1. Using Eq. 2 was utilized to calculate the adsorption capacity at each period (the CIP or OXY milligrams adsorbed onto one gram of sorbent, $q_t$, mg $g^{-1}$).

$$C_t = \frac{Absorbance_{sample}}{Absorbance_{standard}} \times conc._{standard} \quad (1)$$

$$q_t = \frac{(C_o - C_t)\,V}{m}, \quad (2)$$

Fig. 1, 2, 3, and 4 demonstrate the adsorption trend of CIP onto $MgAl_2O_4$, 2.5%$MoO_3$@$MgAl_2O_4$, 5%$MoO_3$@$MgAl_2O_4$, and 10%$MoO_3$@$MgAl_2O_4$, respectively, while Fig. 5, 6, 7, and 8 demonstrated the OXY sorption trend of CIP onto the same four sorbents, respectively. The $MgAl_2O_4$, 2.5%$MoO_3$@$MgAl_2O_4$, 5%$MoO_3$@$MgAl_2O_4$, and 10%$MoO_3$@$MgAl_2O_4$ showed $q_t$ values for CIP were 137.0, 169.2, 190.9 and 156.0 mg $g^{-1}$, respectively, while for OXY they showed $q_t$ values of 121.4, 128.3, 153.9 and 128.4 mg $g^{-1}$, respectively. The CIP sorption reached its equilibrium at 60 minutes, while 30 minutes was sufficient for OXY sorption equilibration onto

the four sorbents. It is worth mentioning that 90% of the gained CIP and OXY $q_t$ values were acquired within the first 20 and 10 minutes, respectively.

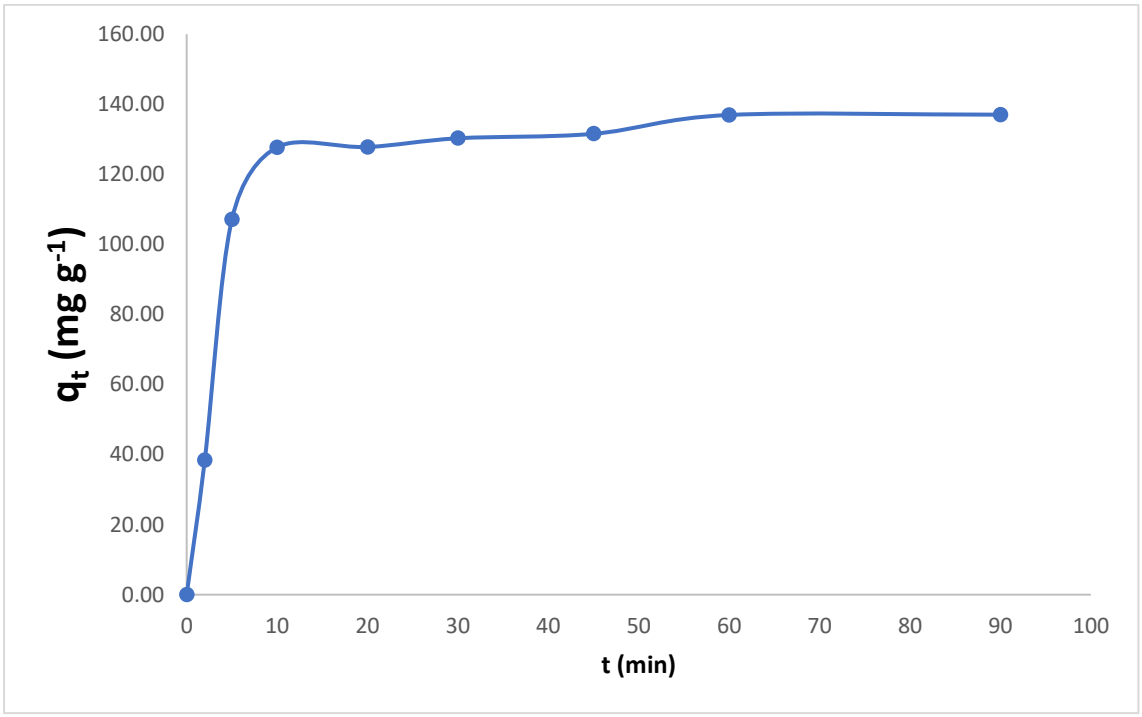


**Fig. 1 The contact time trend of CIP sorption onto the $MgAl_2O_4$ nanocomposite.**

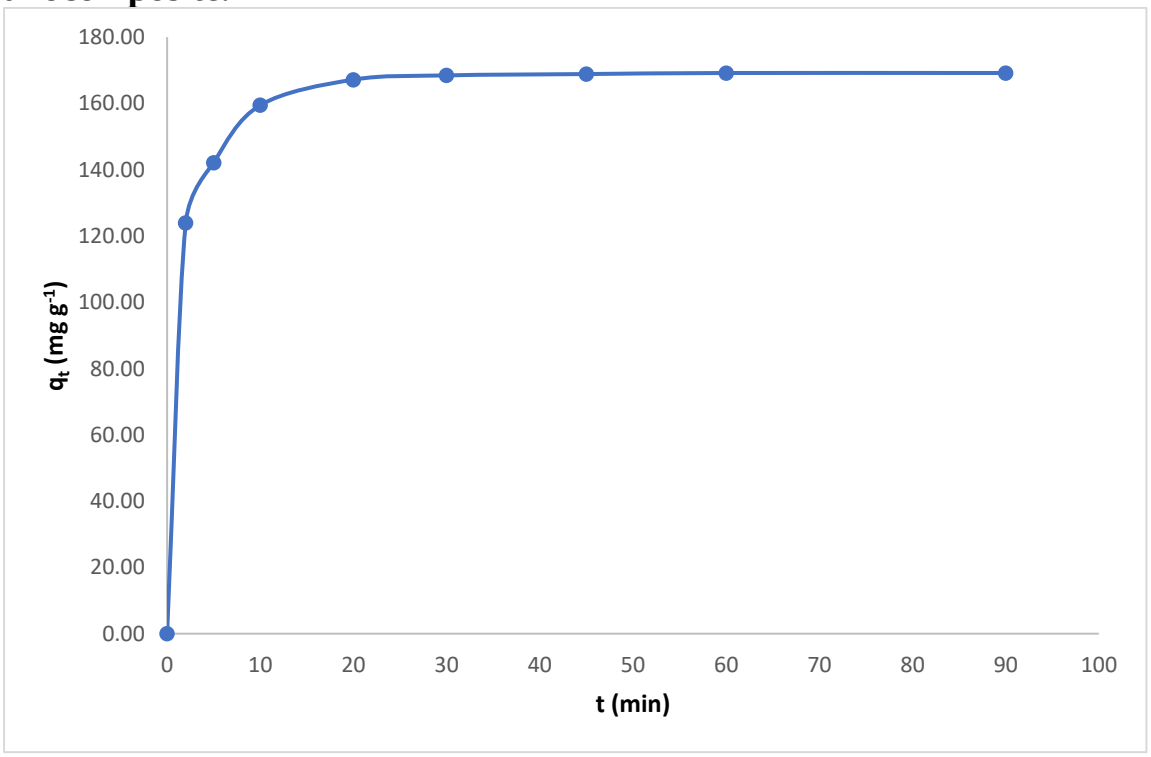


**Fig. 2 The contact time trend of CIP sorption onto the 2.5%$MoO_3$@$MgAl_2O_4$ composite.**

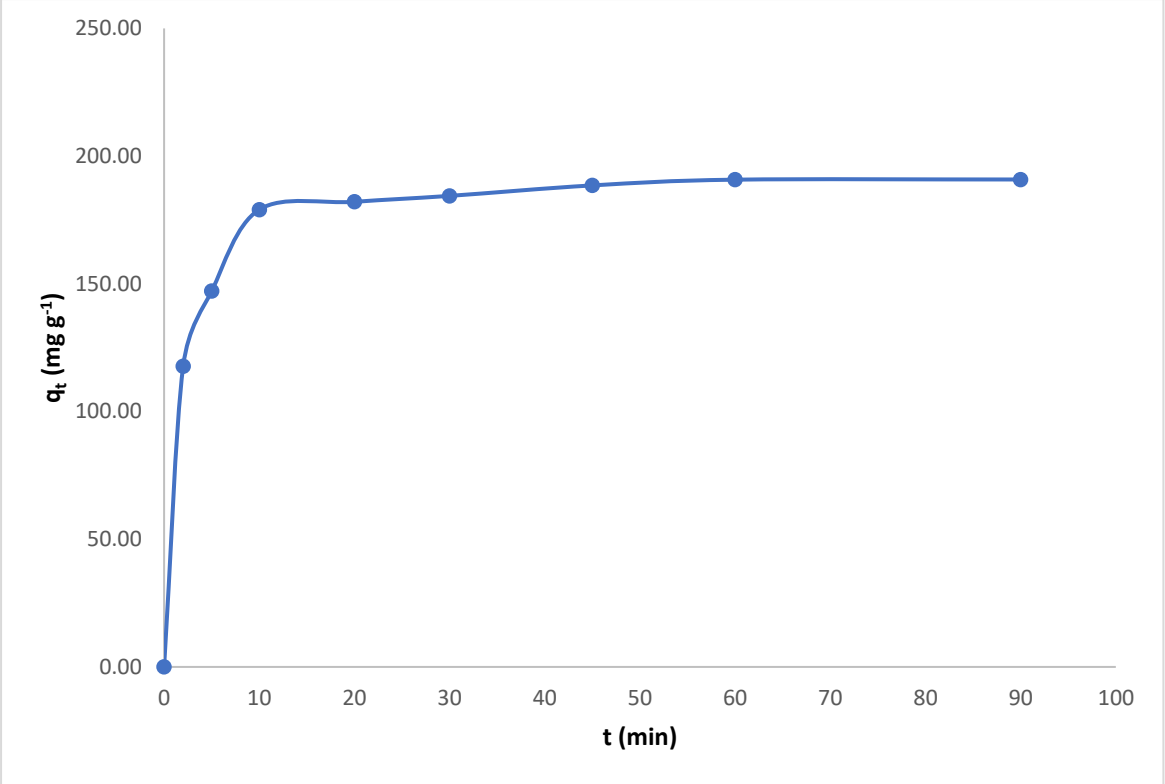


**Fig. 3 The contact time trend of CIP sorption onto the 5%$MoO_3$@$MgAl_2O_4$ composite.**

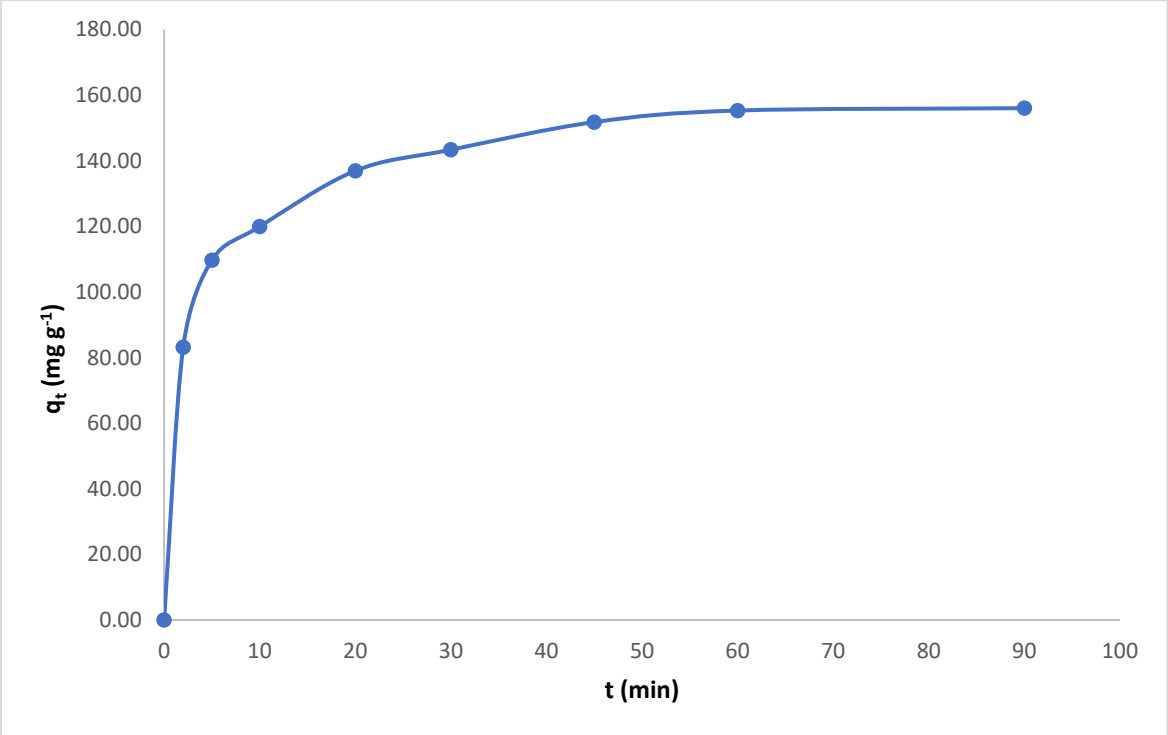


**Fig. 4 The contact time trend of CIP sorption onto the 10%$MoO_3$@$MgAl_2O_4$ composite.**

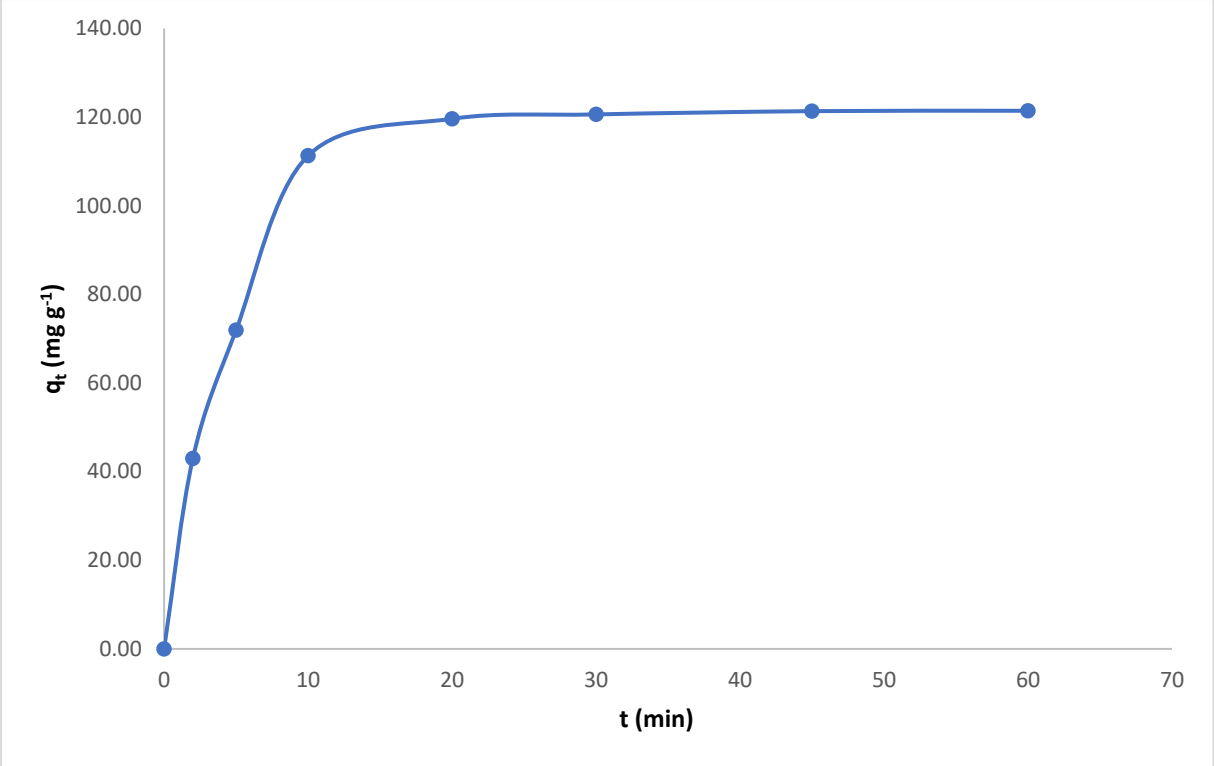


**Fig. 5 The contact time trend of OXY sorption onto the $MgAl_2O_4$ nanocomposite.**

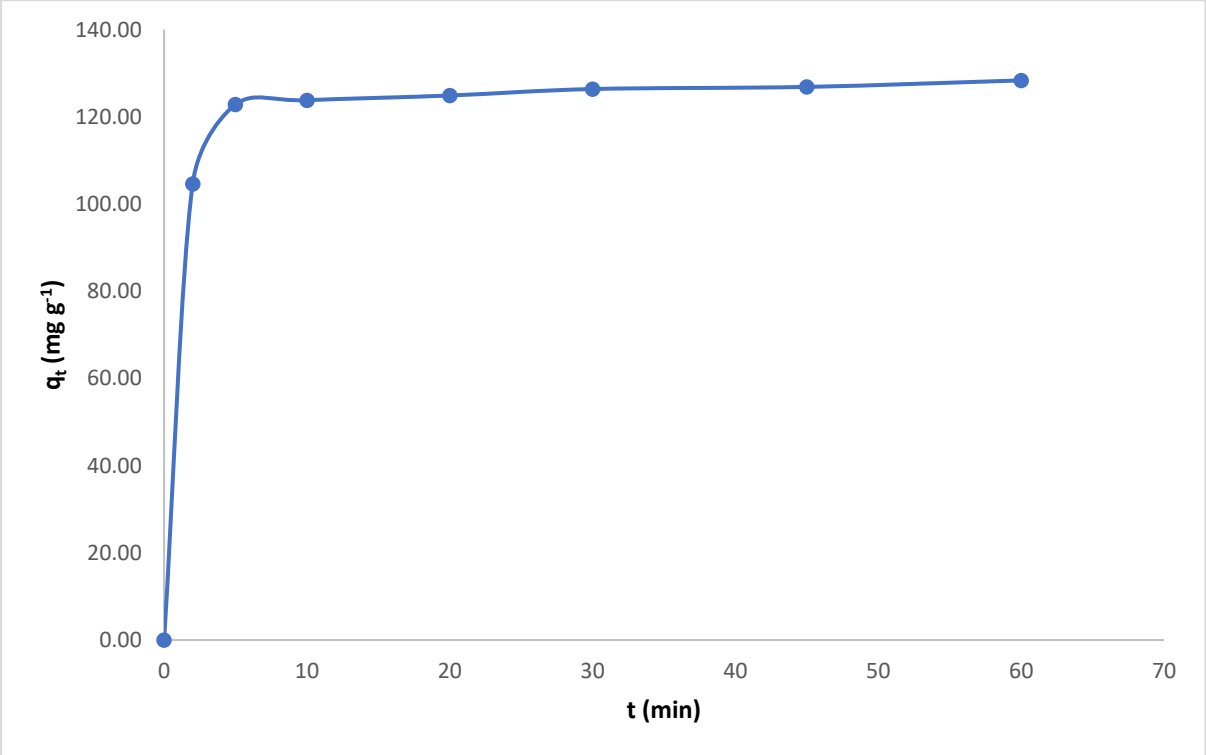


**Fig. 6 The contact time trend of OXY sorption onto the 2.5%$MoO_3$@$MgAl_2O_4$ composite.**

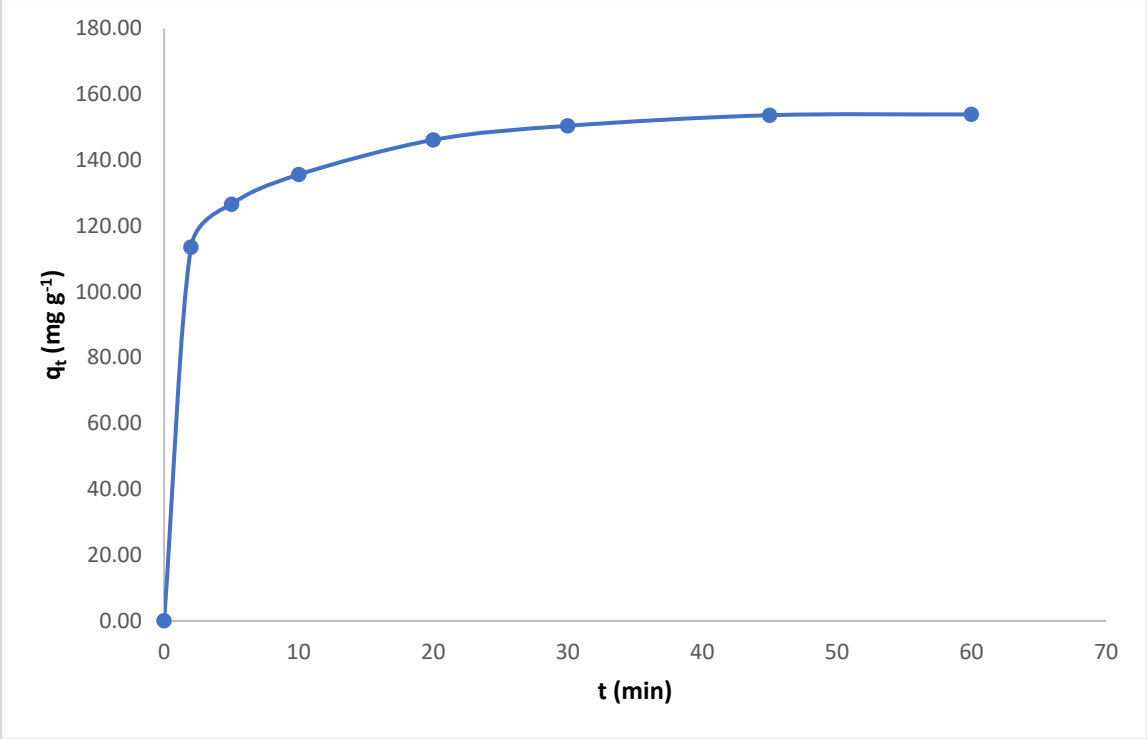


**Fig. 7 The contact time trend of OXY sorption onto the 5%$MoO_3$@$MgAl_2O_4$ composite.**

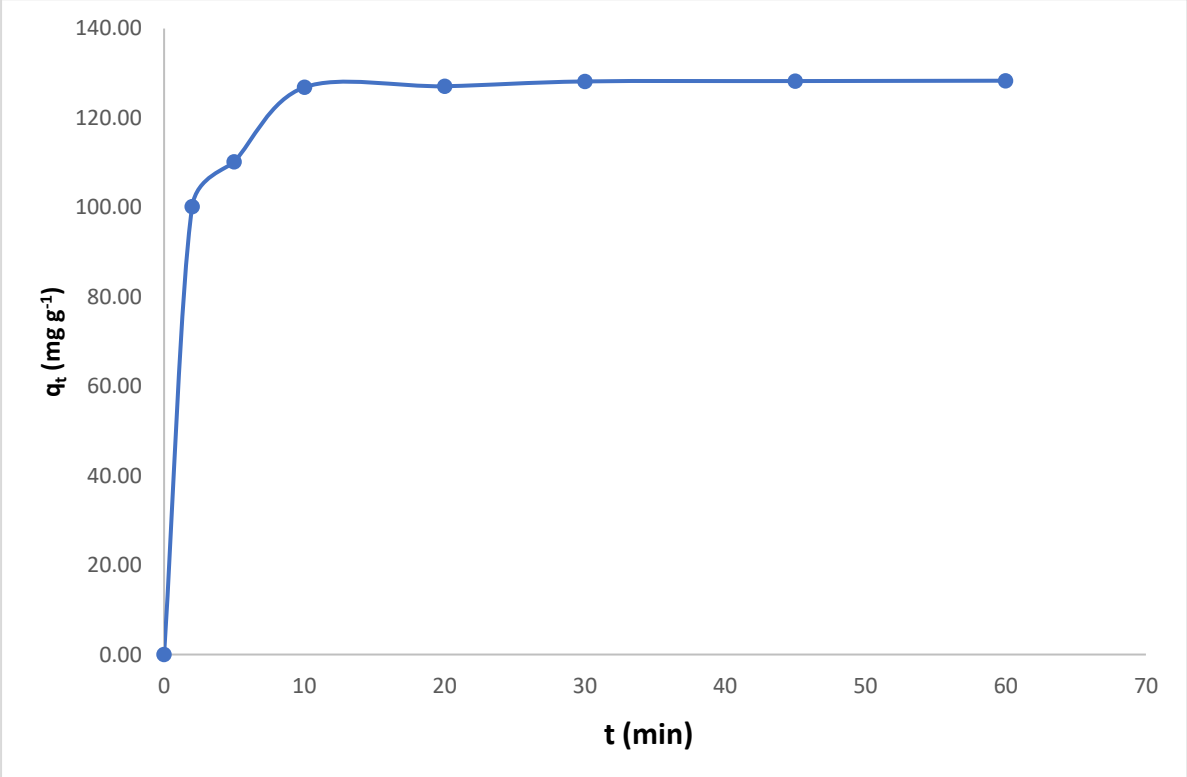


**Fig. 8 The contact time trend of OXY sorption onto the 10%$MoO_3$@$MgAl_2O_4$ composite.**

### 3.2 Adsorption rate order

The adsorption rate order of CIP and OXY removal by $MgAl_2O_4$, 2.5%$MoO_3$@$MgAl_2O_4$, 5%$MoO_3$@$MgAl_2O_4$, and 10%$MoO_3$@$MgAl_2O_4$ was studied via pseudo-first-order (PF, Eq. 3) and pseudo-second-order (PS, Eq. 4) kinetic models.

$$\ln(q_e - q_t) = \ln q_e - k_1.t \quad (3)$$

$$\frac{1}{q_t} = \frac{1}{k_2.q_e^2 t} + \frac{1}{q_e} \quad (4)$$

The symbol $q_e$ (mg g-1) represents the equilibrium adsorption capacity. The PF and PS constants are also time-dependent, with the former represented as k1 ($min^{-1}$) and the latter as k2 (g $mg^{-1}$ $min^{-1}$). The PF plots of the CIP adsorption onto $MgAl_2O_4$, 2.5%$MoO_3$@$MgAl_2O_4$, 5%$MoO_3$@$MgAl_2O_4$, and 10%$MoO_3$@$MgAl_2O_4$ composites were depicted in Fig. 9, 10, 11, and 12, respectively. Fig. 13, 14, 15, and 16 showed the PF plots of OXTC removal by $MgAl_2O_4$, 2.5%$MoO_3$@$MgAl_2O_4$, 5%$MoO_3$@$MgAl_2O_4$, and 10%$MoO_3$@$MgAl_2O_4$, respectively. Additionally, Fig.17, 18, 19, and 20 illustrated the PS plots of CIP sorption onto $MgAl_2O_4$, 2.5%$MoO_3$@$MgAl_2O_4$, 5%$MoO_3$@$MgAl_2O_4$, and 10%$MoO_3$@$MgAl_2O_4$, respectively, while Fig. 21, 22, 23, and 24 showed the PS plots of OXY, respectively. The rate-order output of CIP removal (Table 1) illustrated that the sorption on $MgAl_2O_4$, 2.5%$MoO_3$@$MgAl_2O_4$, and 5%$MoO_3$@$MgAl_2O_4$ fitted the PS; conversely, the sorption on 10%$MoO_3$@$MgAl_2O_4$ followed the PF. Additionally, the OXY rate

investigation output (Table 2) revealed the agreement of OXY sorption onto the four sorbents to the PS, except for the 2.5%$MoO_3$@$MgAl_2O_4$, which fitted the PF.

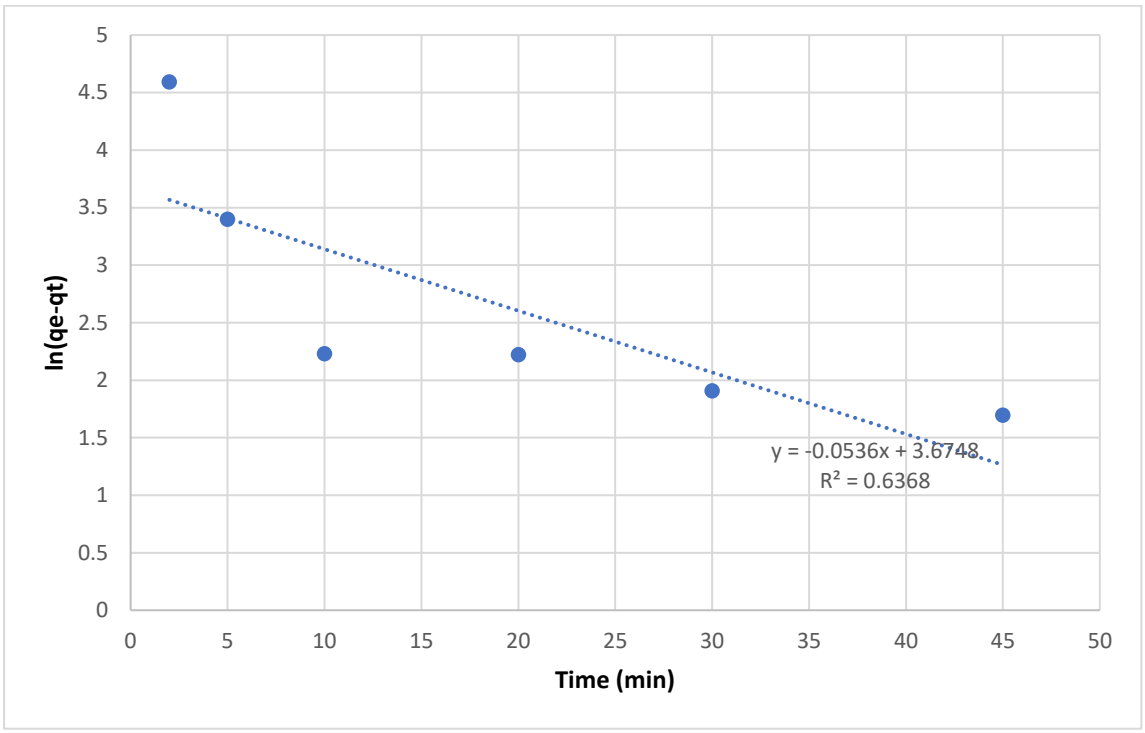


**Fig. 9 The PF investigation of CIP sorption onto $MgAl_2O_4$ composite.**

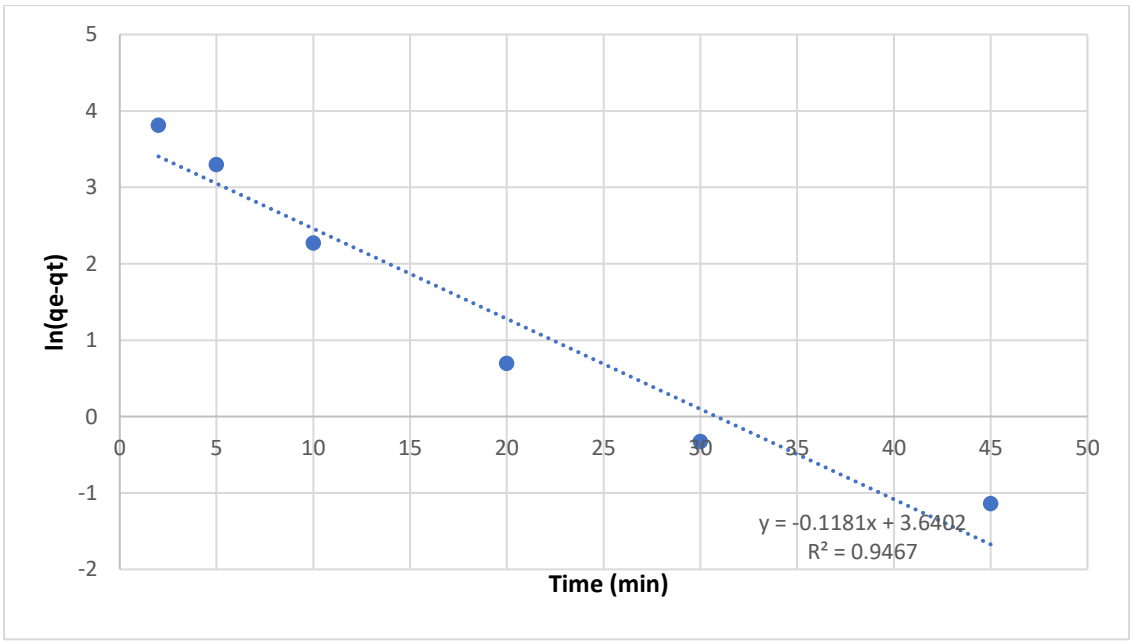


**Fig. 10 The PF investigation of CIP sorption onto 2.5%$MoO_3$@$MgAl_2O_4$ composite.**

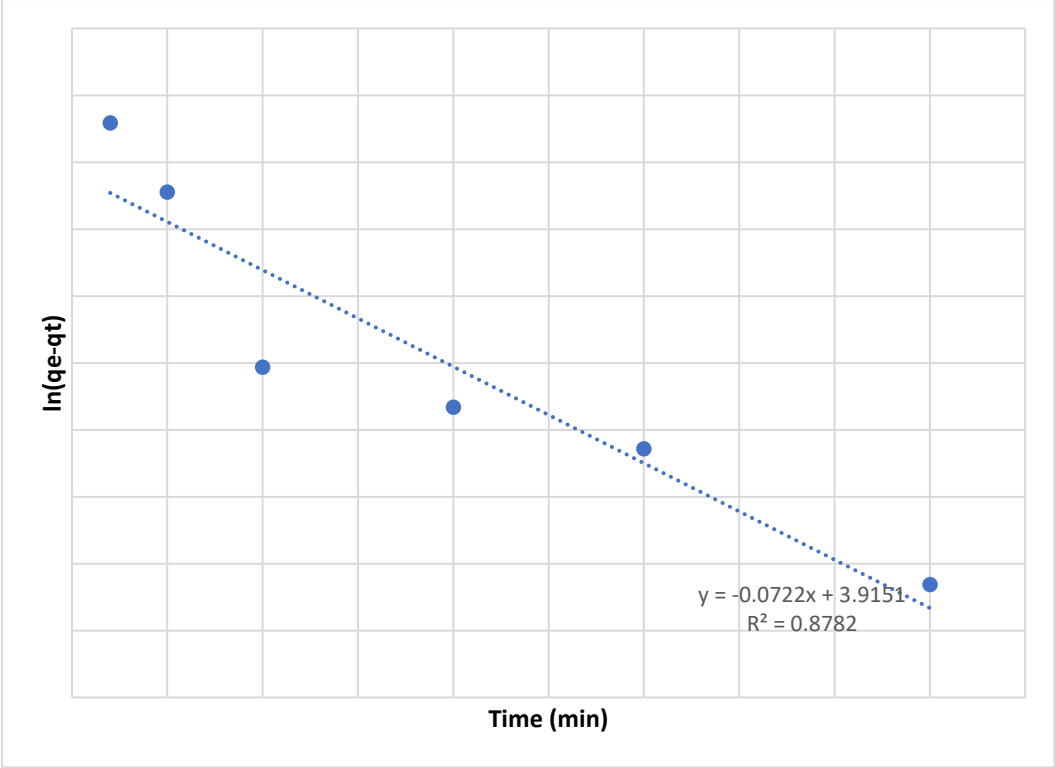


**Fig. 11 The PF investigation of CIP sorption onto $5\%MoO_3@MgAl_2O_4$ composite.**

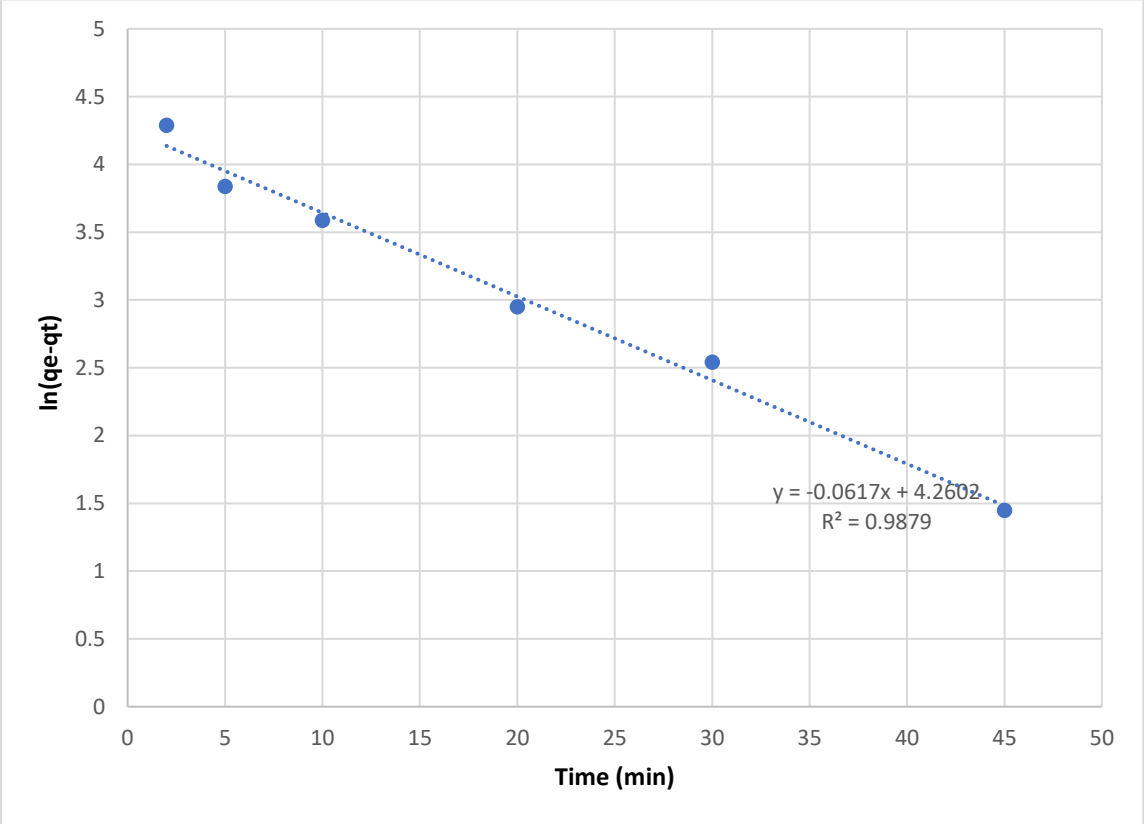


**Fig. 12 The PF investigation of CIP sorption onto $10\%MoO_3@MgAl_2O_4$ composite.**

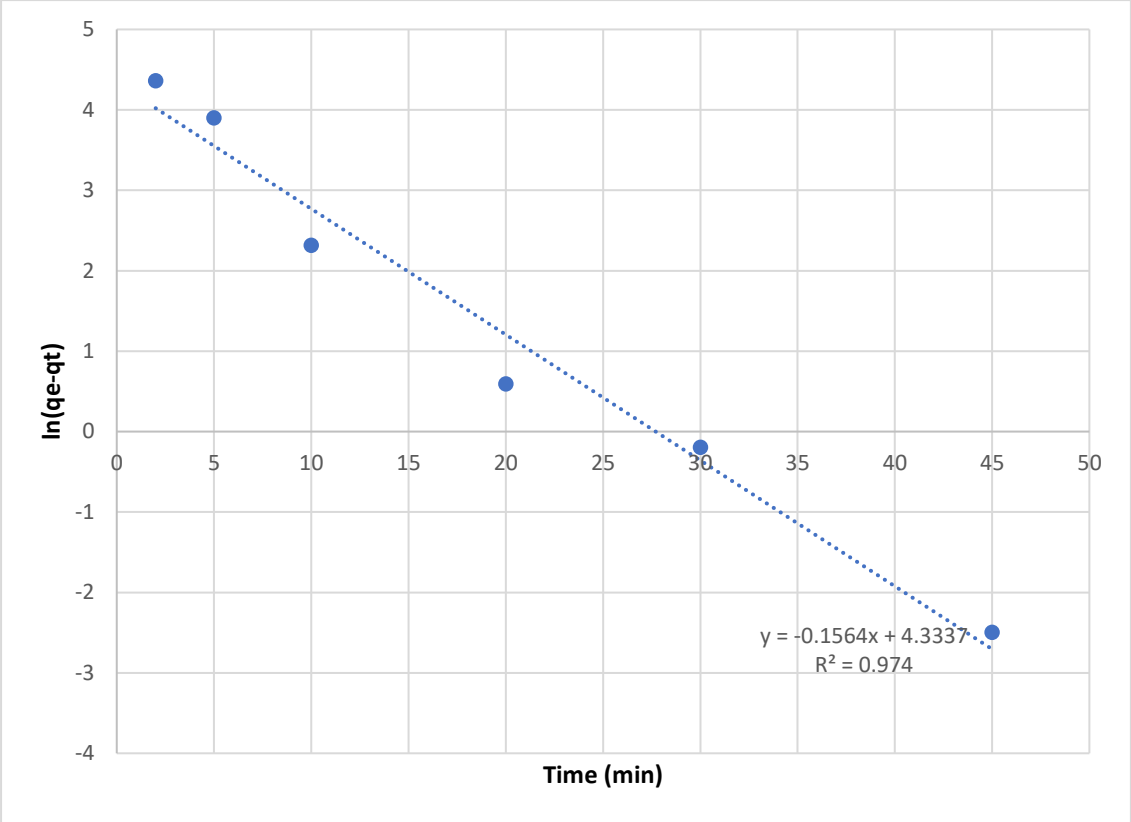


**Fig. 13 The PF investigation of OXY sorption onto $MgAl_2O_4$ composite.**

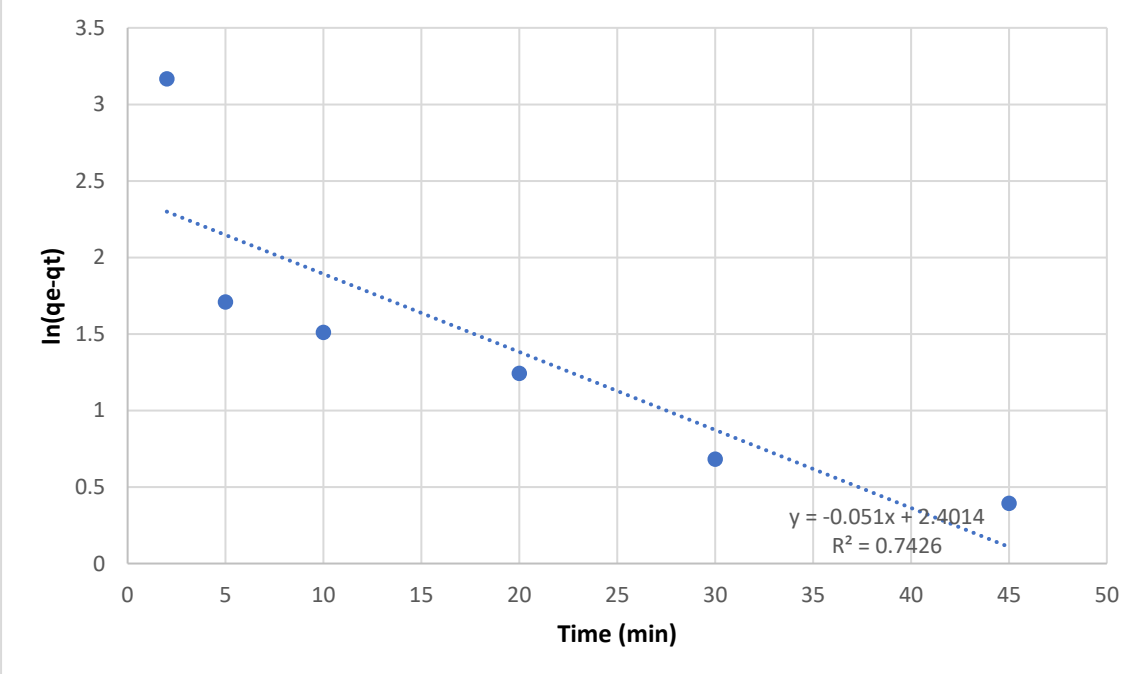


**Fig. 14 The PF investigation of OXY sorption onto $2.5\%MoO_3@MgAl_2O_4$ composite.**

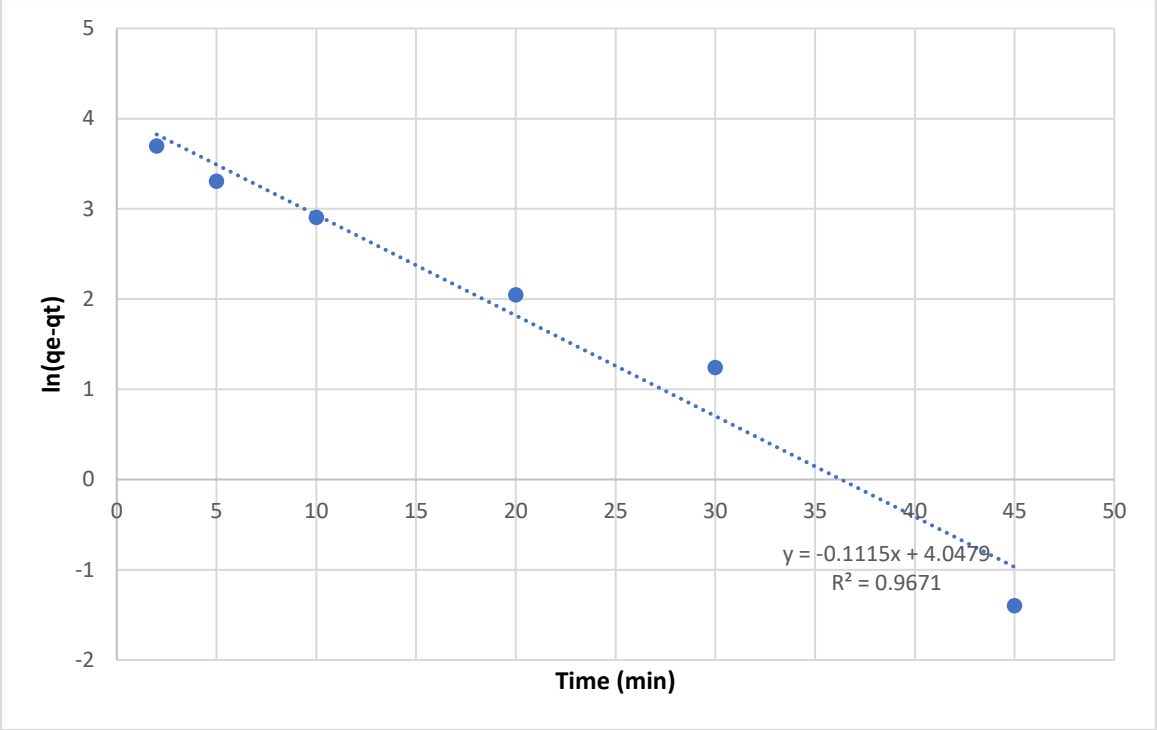


**Fig. 15 The PF investigation of OXY sorption onto 5%$MoO_3$@$MgAl_2O_4$ composite.**

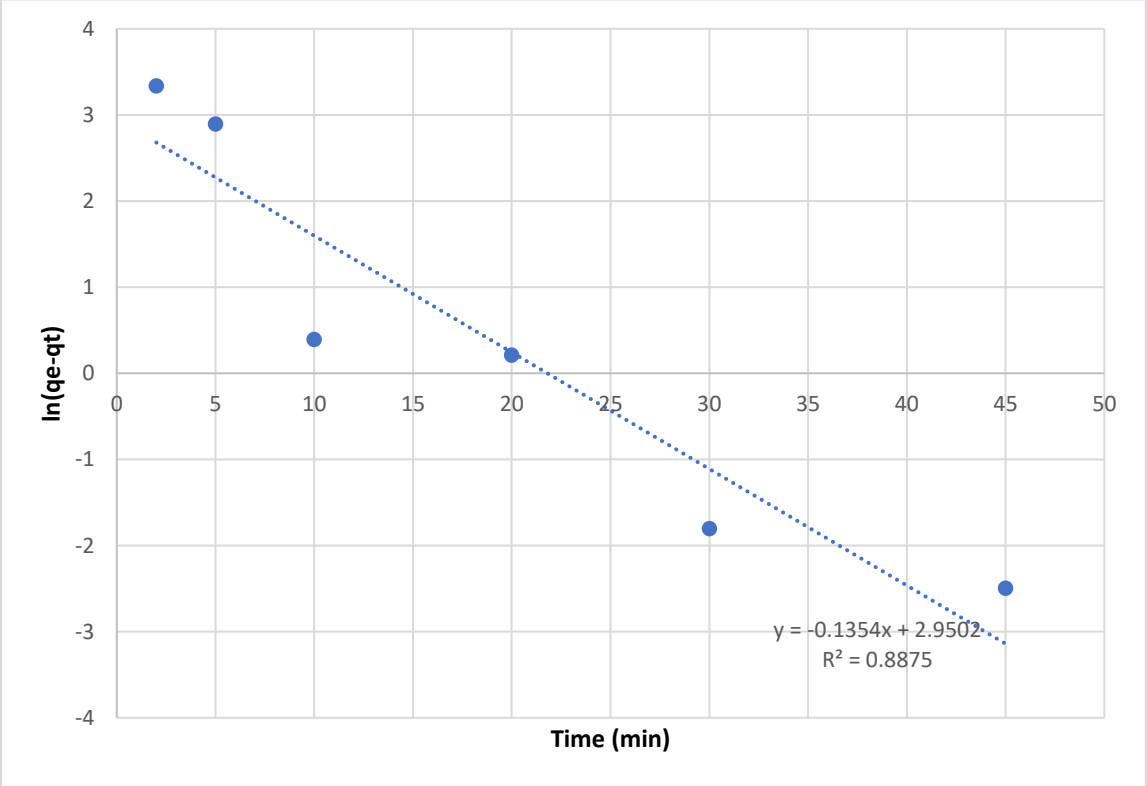


**Fig. 16 The PF investigation of OXY sorption onto 10%$MoO_3$@$MgAl_2O_4$ composite.**

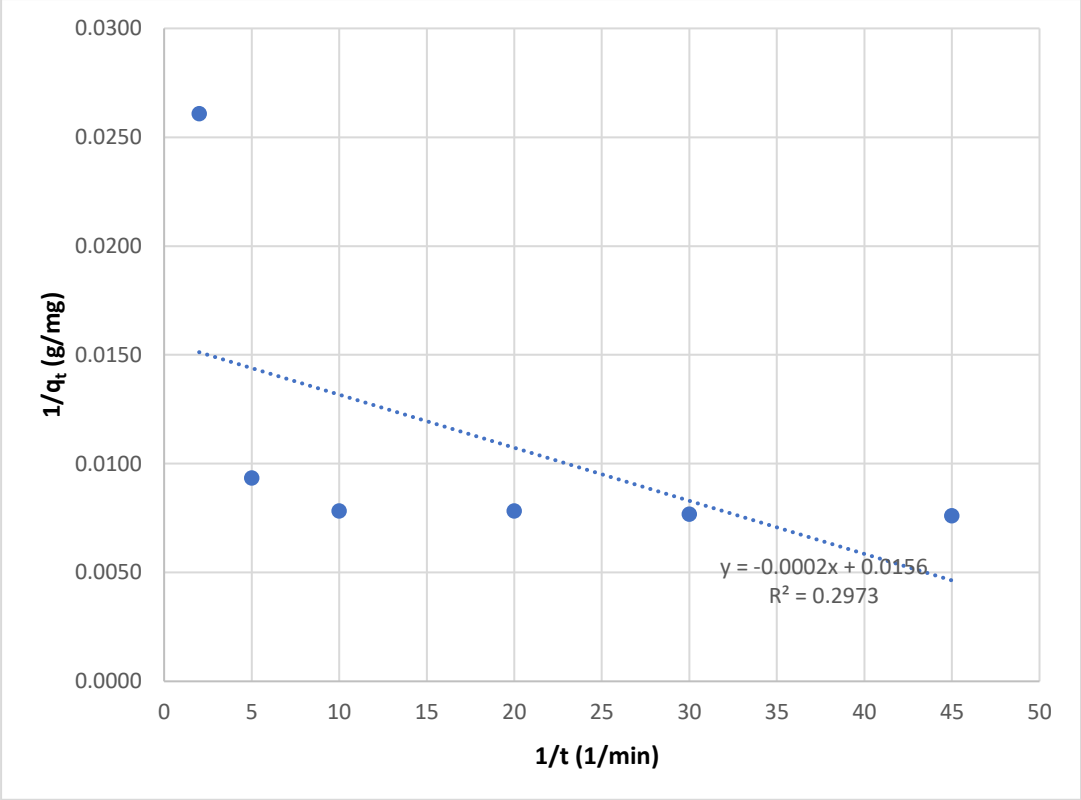


**Fig. 17 The PS investigation of CIP sorption onto $MgAl_2O_4$ composite.**

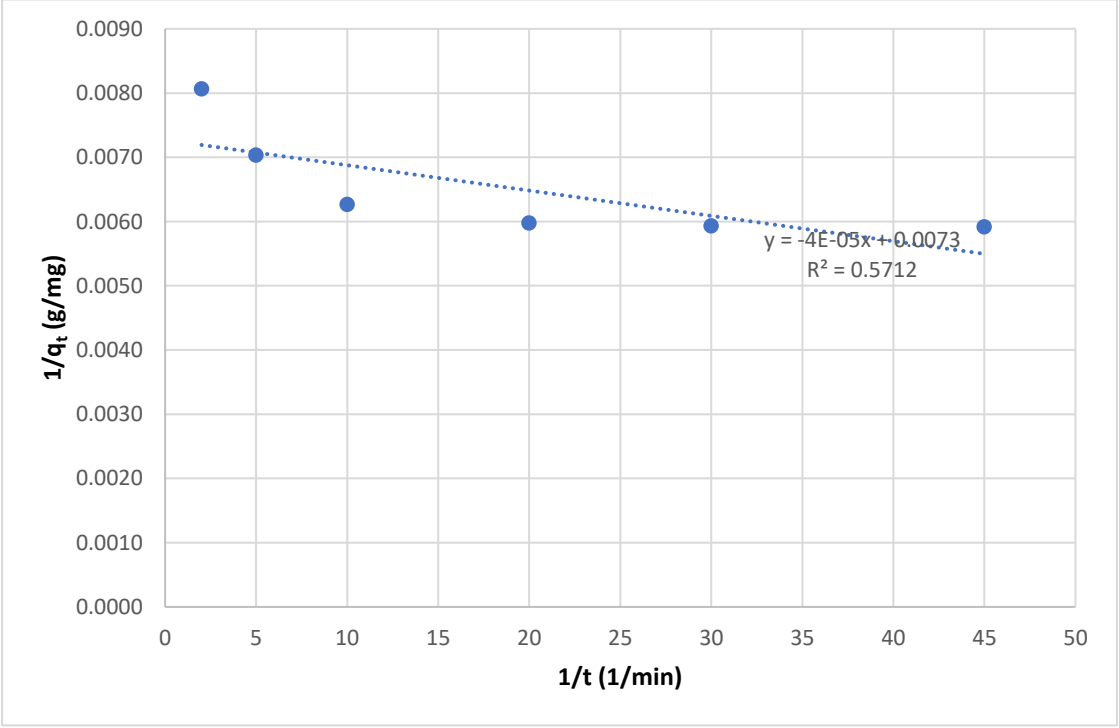


**Fig. 18 The PS investigation of CIP sorption onto $2.5\%MoO_3@MgAl_2O_4$ composite.**

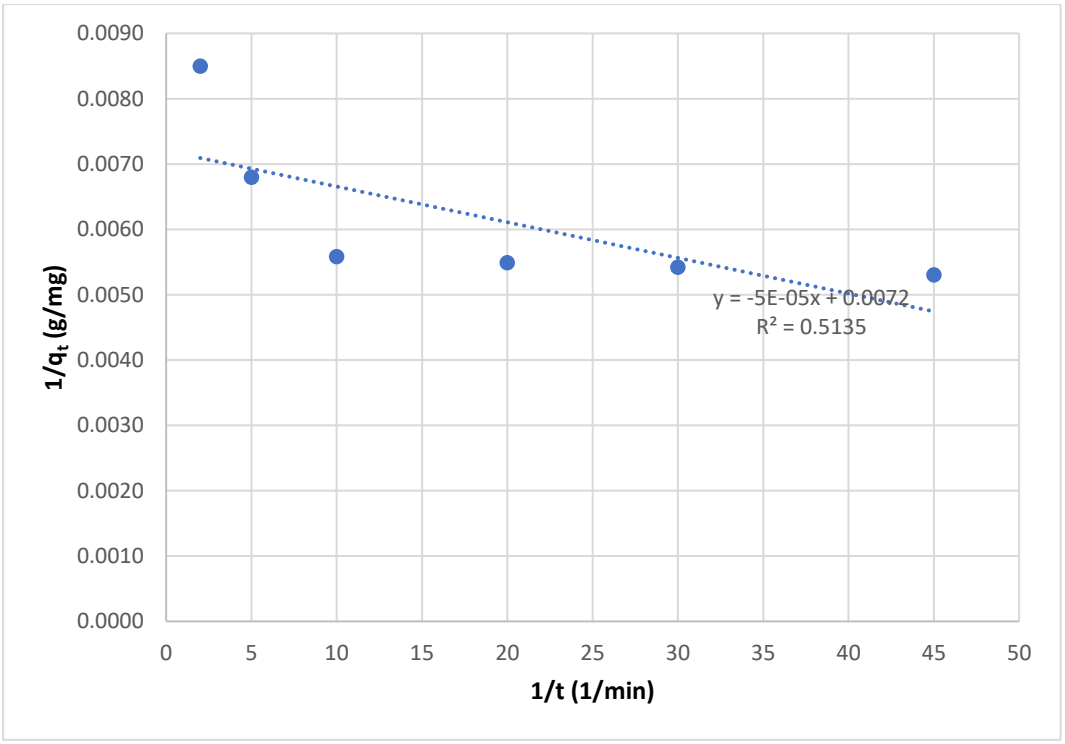


**Fig. 19 The PS investigation of CIP sorption onto $5\%MoO_3@MgAl_2O_4$ composite.**

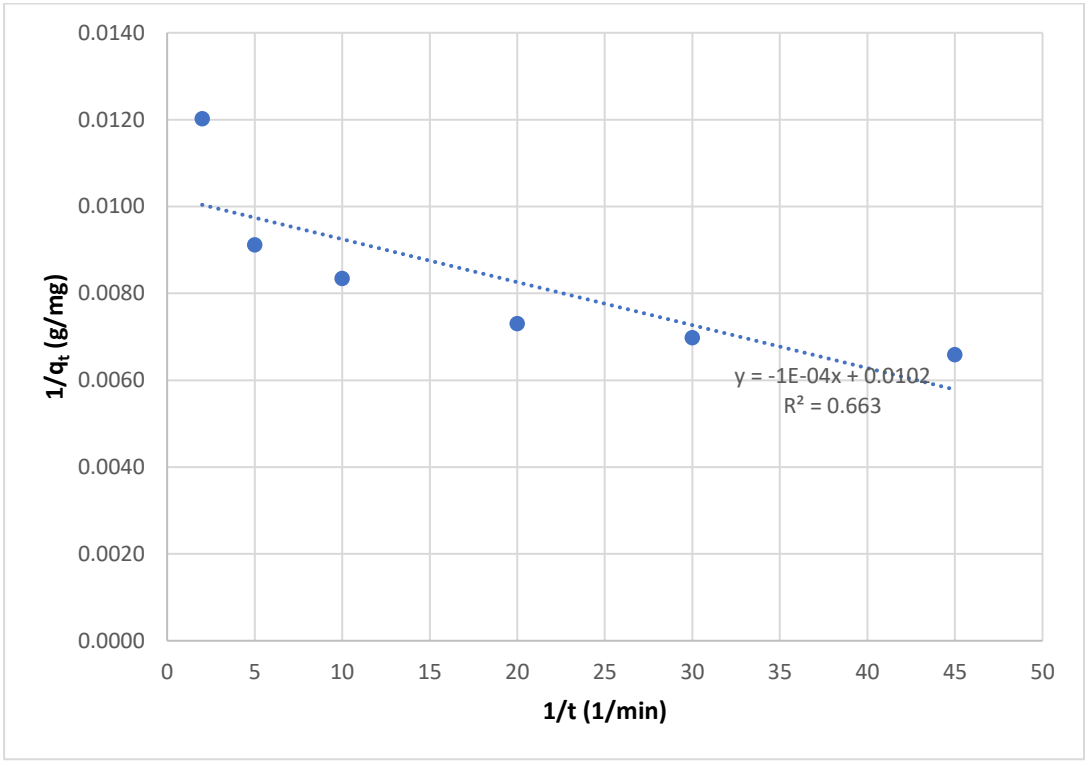


**Fig. 20 The PS investigation of CIP sorption onto $10\%MoO_3@MgAl_2O_4$ composite.**

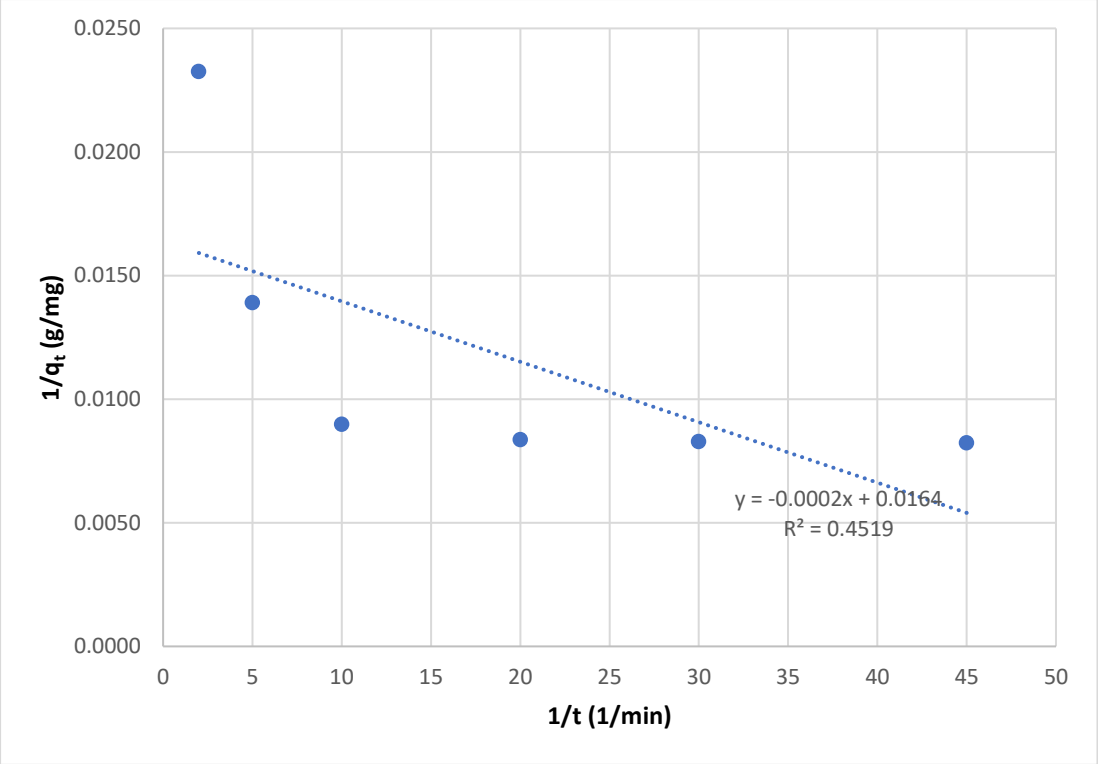


**Fig. 21 The PS investigation of OXY sorption onto $MgAl_2O_4$ composite.**

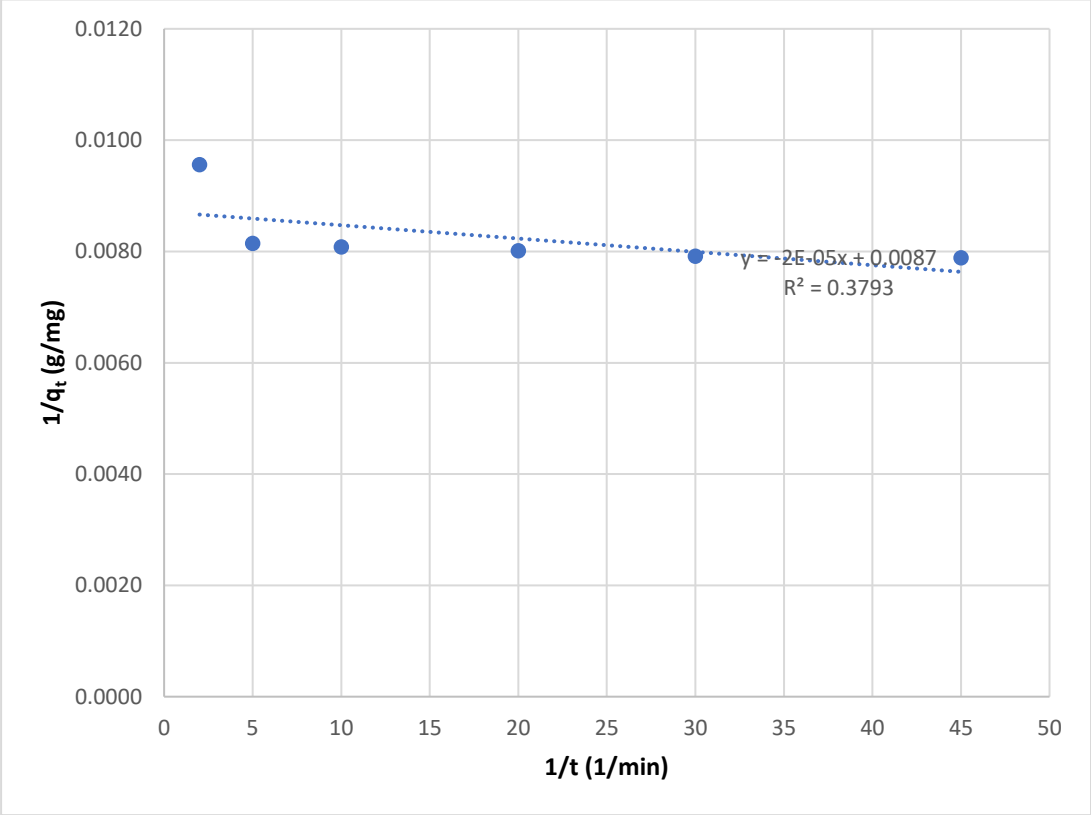


**Fig. 22 The PS investigation of OXY sorption onto $2.5\%MoO_3@MgAl_2O_4$ composite.**

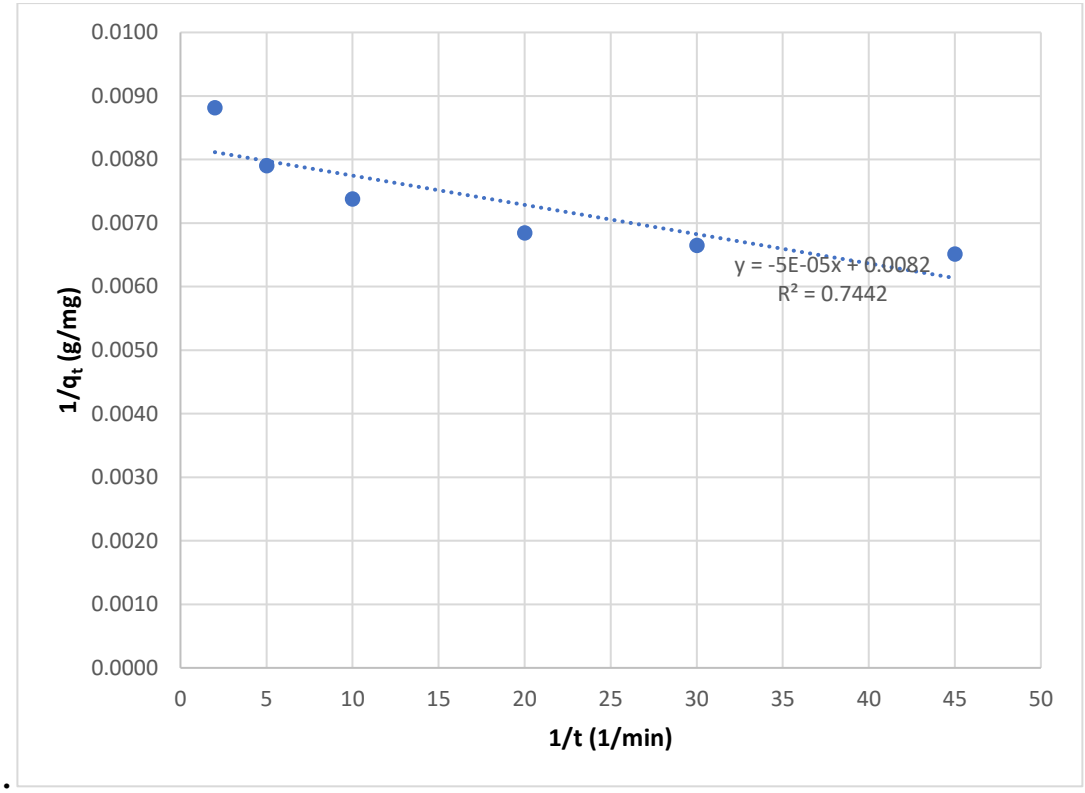


**Fig. 23 The PS investigation of OXY sorption onto $5\%MoO_3@MgAl_2O_4$ composite.**

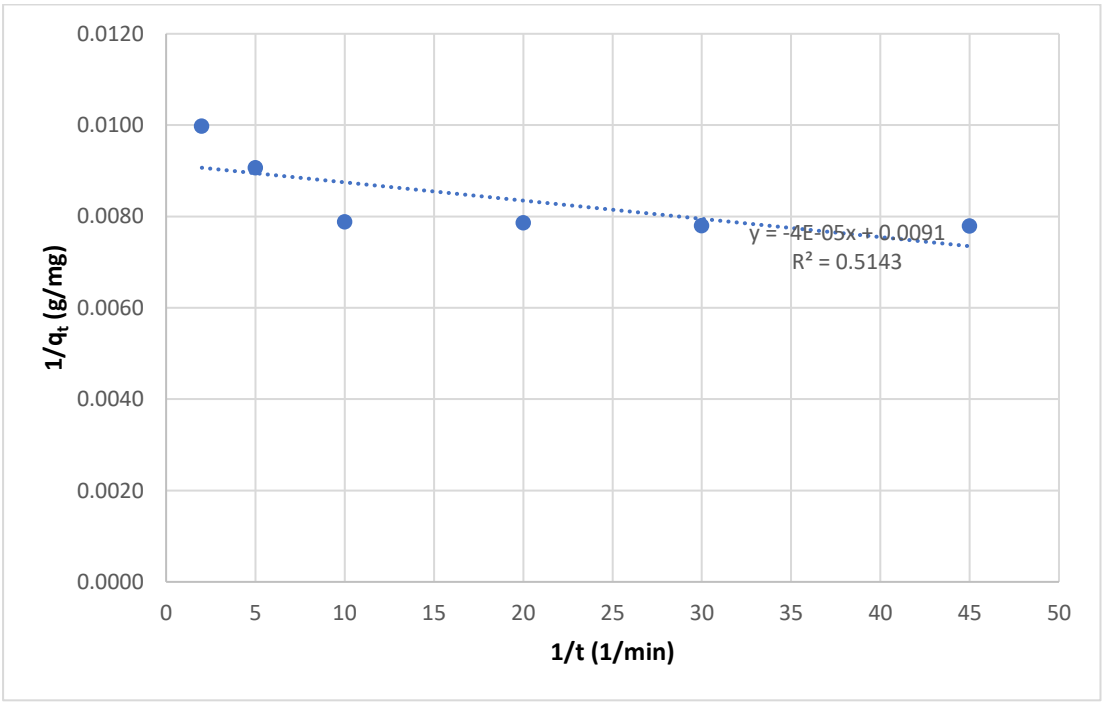


**Fig. 24 The PS investigation of OXY sorption onto $10\%MoO_3@MgAl_2O_4$ composite.**

**Table 1 The adsorption rate order results of CIP removal by $MgAl_2O_4$, 2.5%$MoO_3$@$MgAl_2O_4$, 5%$MoO_3$@$MgAl_2O_4$, and 10%$MoO_3$@$MgAl_2O_4$.**

| Adsorbent | qe exp. (mg $g^{-1}$) | *PFO* | | *PSO* | |
|---|---|---|---|---|---|
| | | $R^2$ | $k_1$ | $R^2$ | $k_2$ |
| AlMgO4 | 137.02 | 0.6368 | 0.0536 | 0.9739 | 0.001 |
| 2.5%MoO3@AlMgO4 | 169.19 | 0.9467 | 0.1181 | 0.9783 | 0.007 |
| 5%MoO3@AlMgO4 | 190.85 | 0.8782 | 0.0722 | 0.9872 | 0.004 |
| 10%MoO3@AlMgO4 | 156.04 | 0.9879 | 0.0617 | 0.9658 | 0.004 |

**Table 2 The adsorption rate order results of OXY removal by $MgAl_2O_4$, 2.5%$MoO_3$@$MgAl_2O_4$, 5%$MoO_3$@$MgAl_2O_4$, and 10%$MoO_3$@$MgAl_2O_4$.**

| Adsorbent | qe exp. (mg g-1) | PFO | | PSO | |
|---|---|---|---|---|---|
| | | R2 | k1 | R2 | k2 |
| AlMgO4 | 121.42 | 0.974 | 0.1564 | 0.9435 | 0.001 |
| 2.5%MoO3@AlMgO4 | 128.34 | 0.743 | 0.0510 | 0.9518 | 0.018 |
| 5%MoO3@AlMgO4 | 153.87 | 0.967 | 0.1115 | 0.9929 | 0.009 |
| 10%MoO3@AlMgO4 | 128.34 | 0.888 | 0.1354 | 0.9975 | 0.012 |

### 3.3 Adsorption control mechanism

It is believed that there are two steps to the adsorption process, the first of which is the movement of adsorbate molecules from a liquid to a solid sorbent surface. Step two involves getting the sorbate molecules to go deep into the sorbent. The rate control mechanism, the slowest sorption step, determines the adsorption rate. The rate-control mechanism of CIP and OXY removal by $MgAl_2O_4$, 2.5%$MoO_3$@$MgAl_2O_4$, 5%$MoO_3$@$MgAl_2O_4$, and 10%$MoO_3$@$MgAl_2O_4$ was studied via using the intraparticle (IPD, Eq. 5) and the liquid-film (LFD, Eq. 6) diffusion model.

$$q_t = K_{IP} * t^{\frac{1}{2}} + C_i \quad (5)$$

$$\ln(1 - F) = -K_{LF} * t \quad (6)$$

The IPD constant is denoted by $K_{IPD}$ (mg $g^{-1}$ $min^{-1/2}$), and the LFD constant is designated by $K_{LFD}$ ($min^{-1}$). $C_i$: the boundary layer factor, expressed as mg $g^{-1}$. The LFD plots of the CIP adsorption onto $MgAl_2O_4$, 2.5%$MoO_3$@$MgAl_2O_4$, 5%$MoO_3$@$MgAl_2O_4$, and 10%$MoO_3$@$MgAl_2O_4$ composites were depicted in Fig. 25, 26, 27, and 28, respectively. Fig. 29, 30, 31, and 32 showed the LFD plots of OXTC removal by $MgAl_2O_4$, 2.5%$MoO_3$@$MgAl_2O_4$, 5%$MoO_3$@$MgAl_2O_4$, and 10%$MoO_3$@$MgAl_2O_4$, respectively. Additionally, Fig.33, 34, 35, and 36 illustrated the IPD plots of CIP sorption onto $MgAl_2O_4$, 2.5%$MoO_3$@$MgAl_2O_4$, 5%$MoO_3$@$MgAl_2O_4$, and 10%$MoO_3$@$MgAl_2O_4$,

respectively, while Fig. 37, 38, 39, and 40 showed the IPD plots of OXY, respectively.

The rate-control output of CIP removal (Table 3) illustrated that the LFD controlled the sorption on MgAl2O4, 2.5%MoO3@MgAl2O4, and 5%MoO3@MgAl2O4. Additionally, the OXY rate-control investigation output (Table 4) revealed the agreement of OXY sorption onto the four sorbents to the LFD.

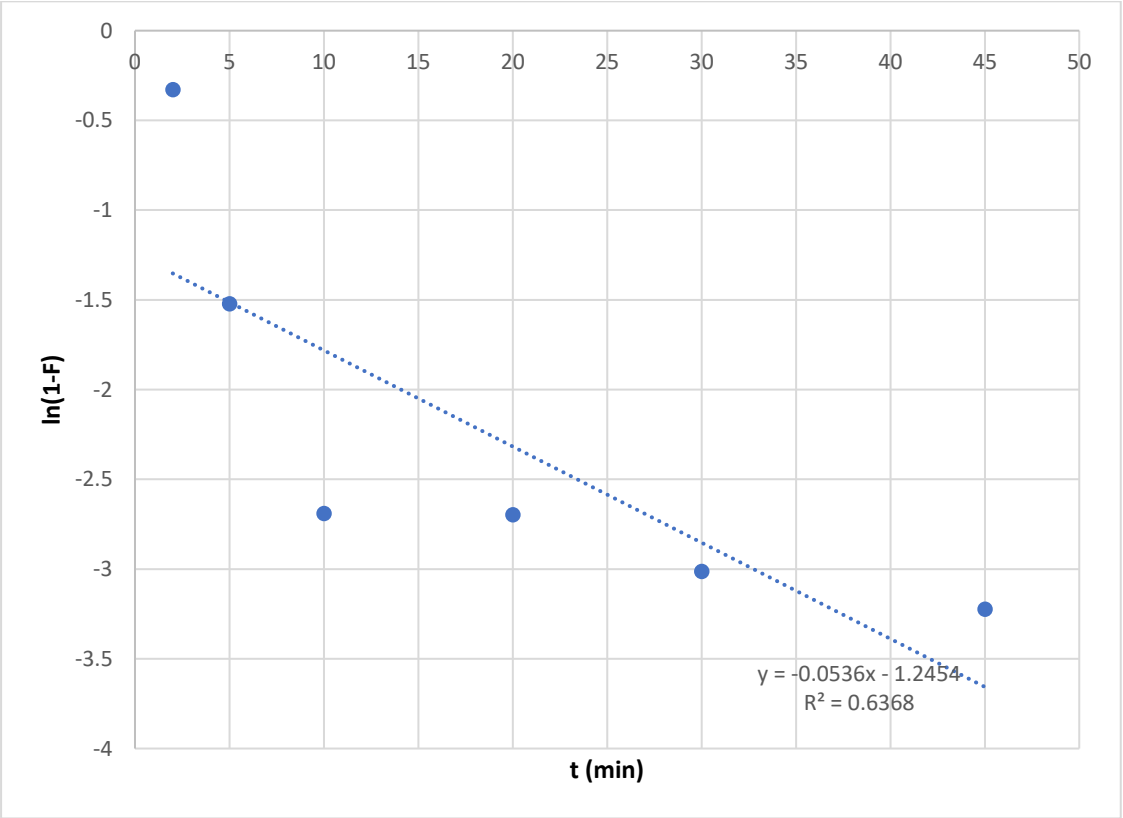


**Fig. 25 The LFD investigation of CIP sorption onto $MgAl_2O_4$ composite.**

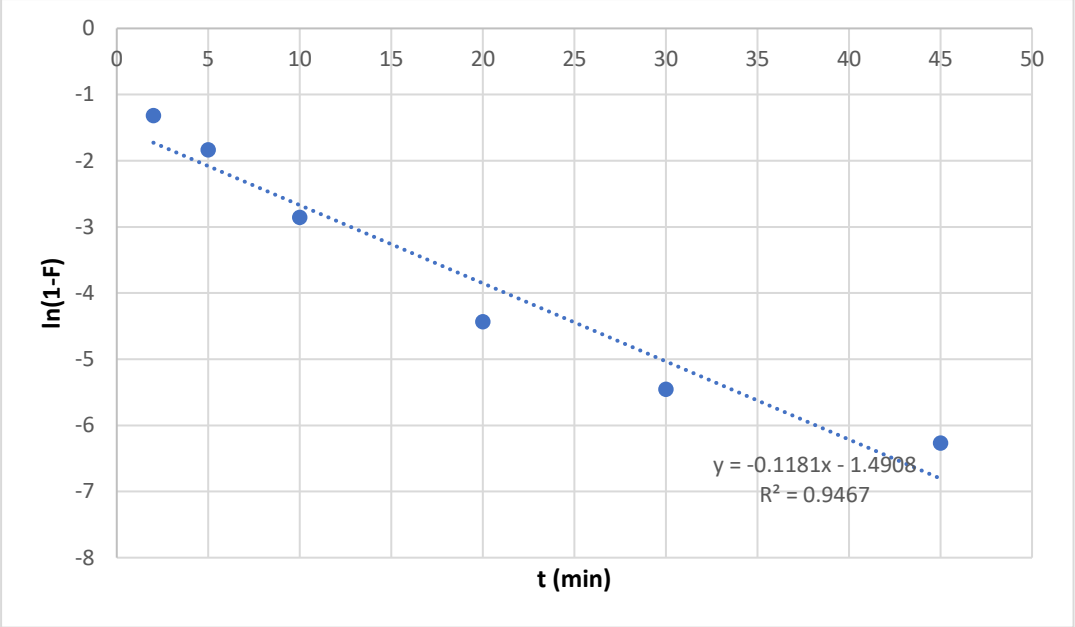


**Fig. 26 The LFD investigation of CIP sorption onto 2.5%$MoO_3$@$MgAl_2O_4$ composite.**

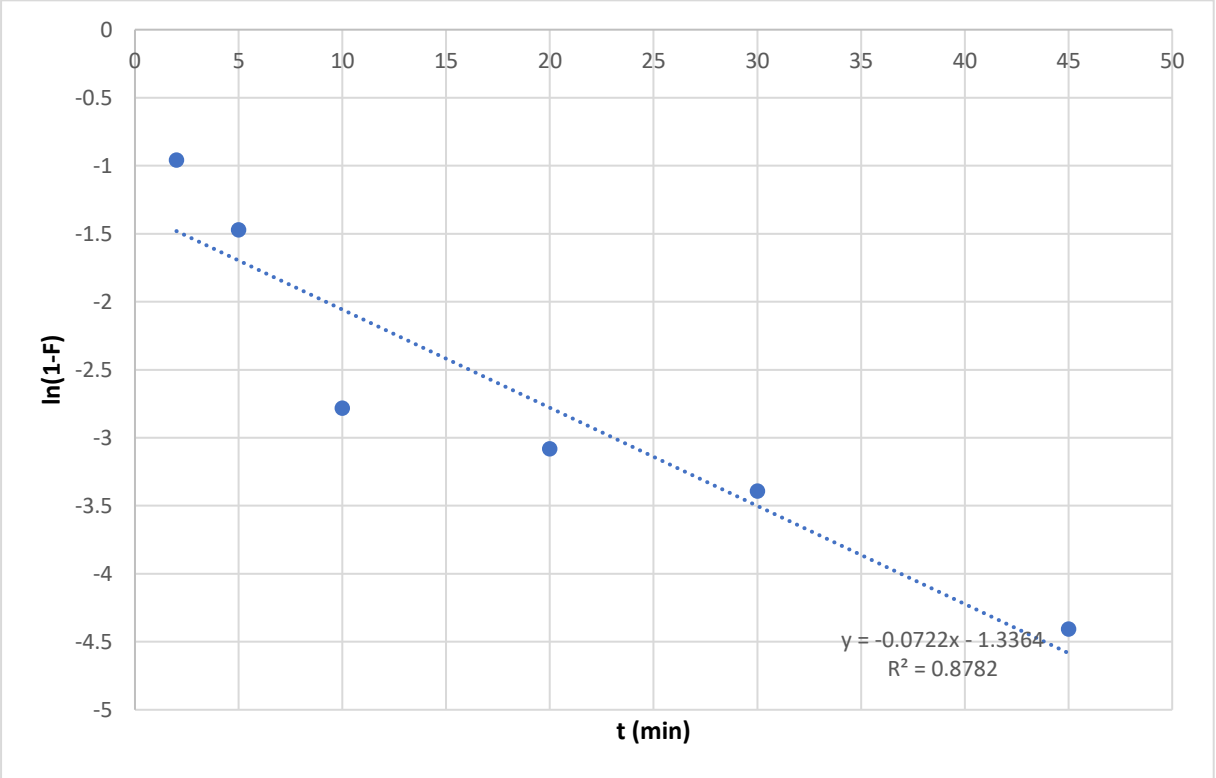


**Fig. 27 The LFD investigation of CIP sorption onto 5%$MoO_3$@$MgAl_2O_4$ composite.**

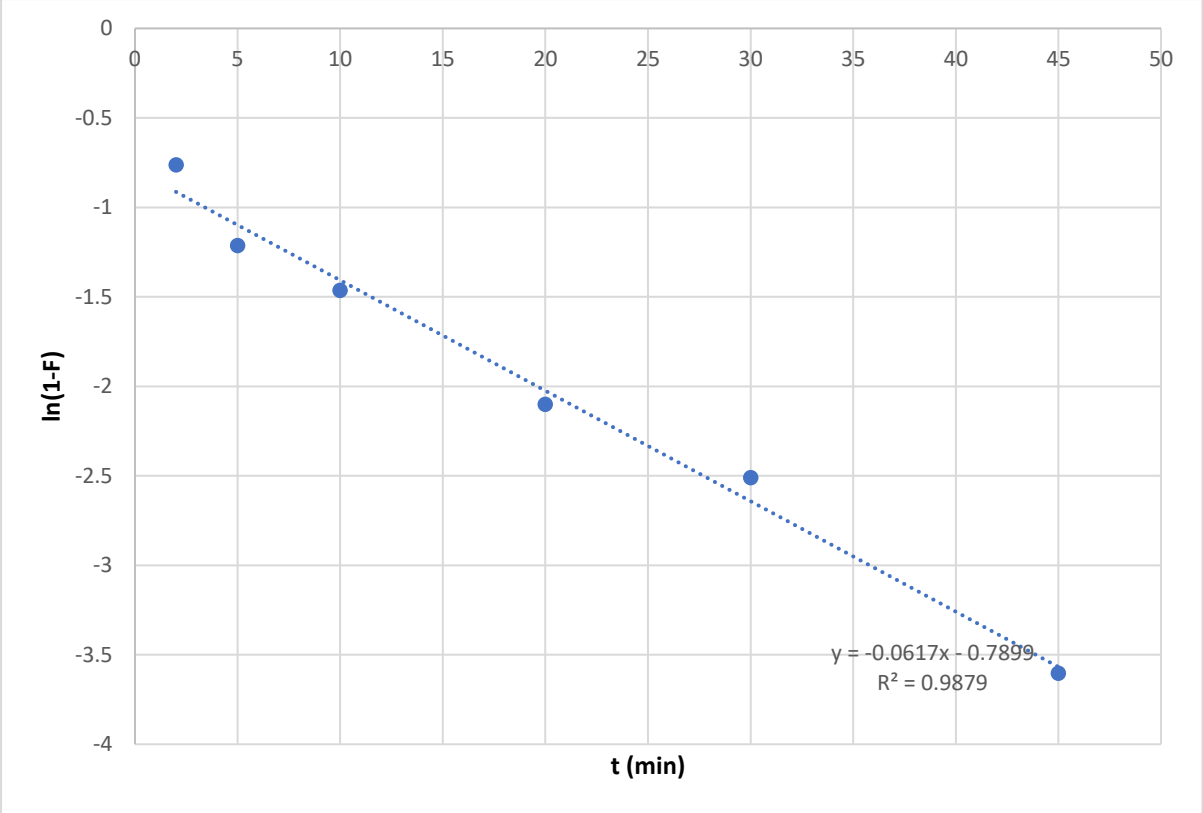


**Fig. 28 The LFD investigation of CIP sorption onto 10%$MoO_3$@$MgAl_2O_4$ composite.**

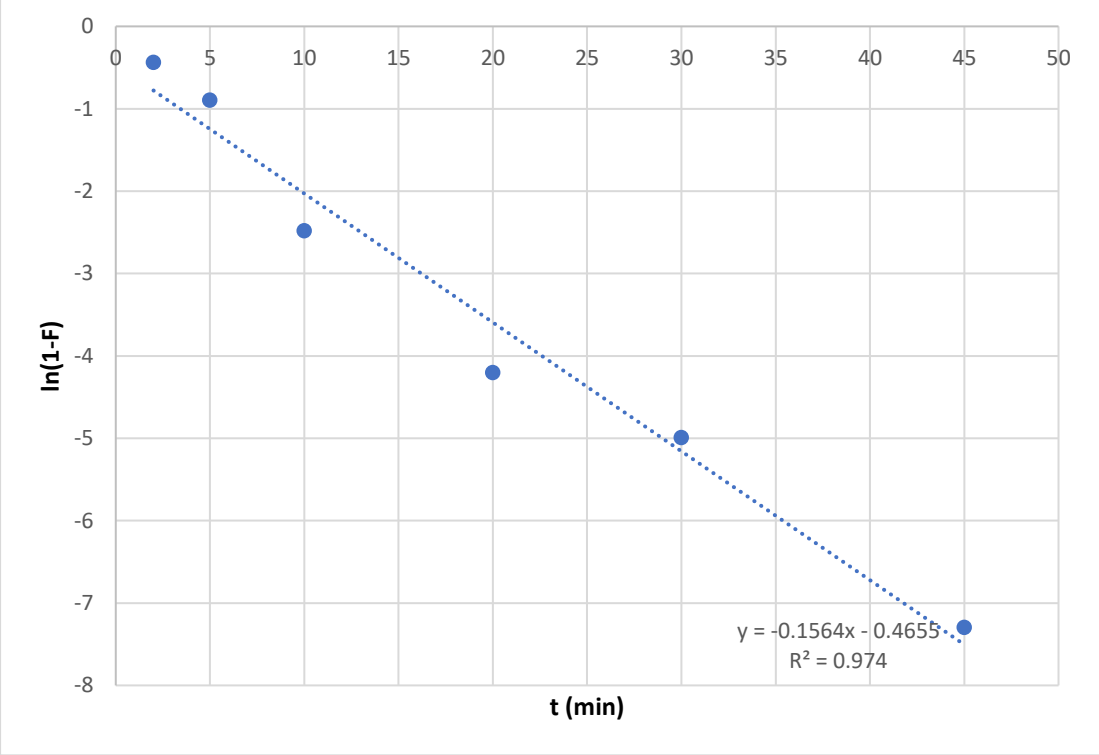


**Fig. 29 The LFD investigation of OXY sorption onto $MgAl_2O_4$ composite.**

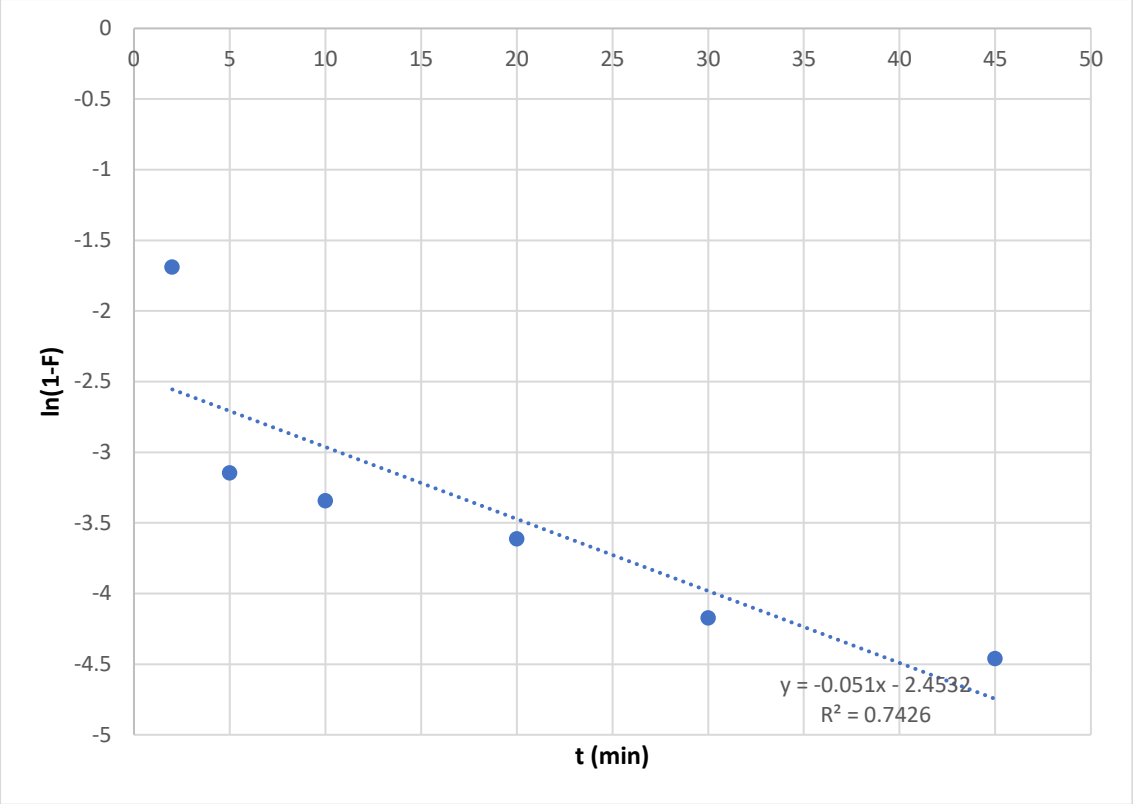


**Fig. 30 The LFD investigation of OXY sorption onto 2.5%$MoO_3$@$MgAl_2O_4$ composite.**

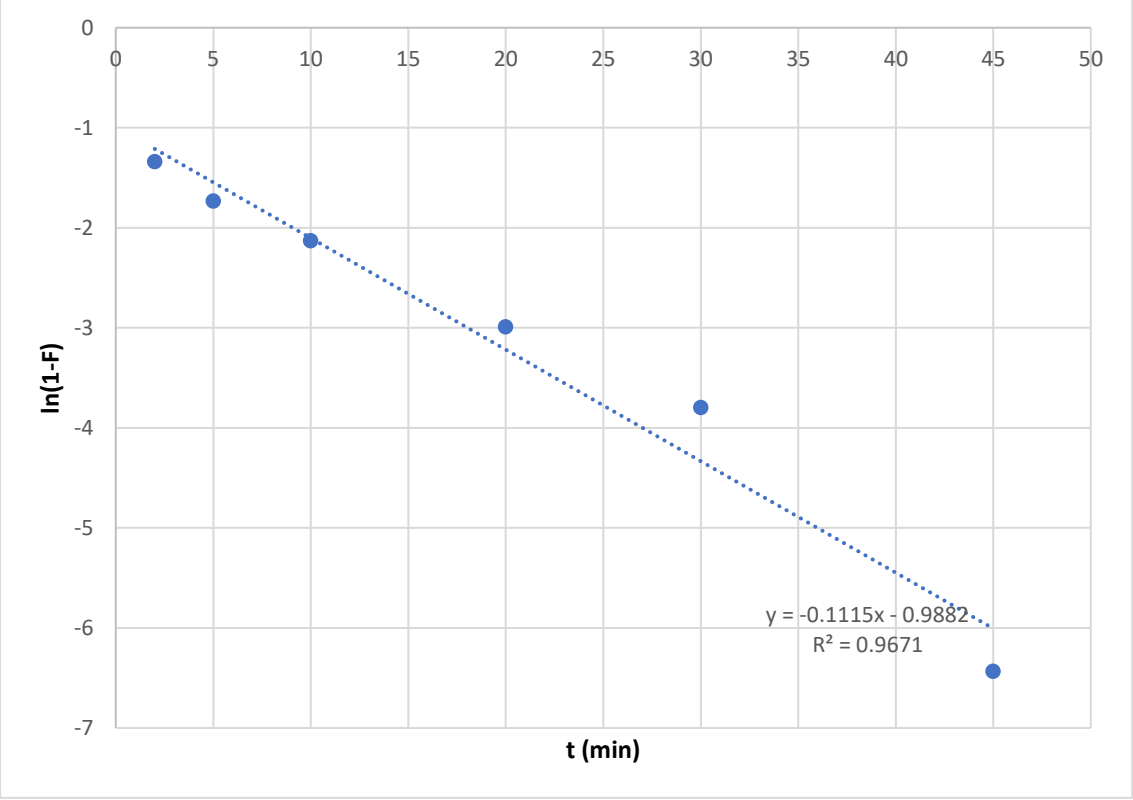


**Fig. 31 The LFD investigation of OXY sorption onto 5%$MoO_3$@$MgAl_2O_4$ composite.**

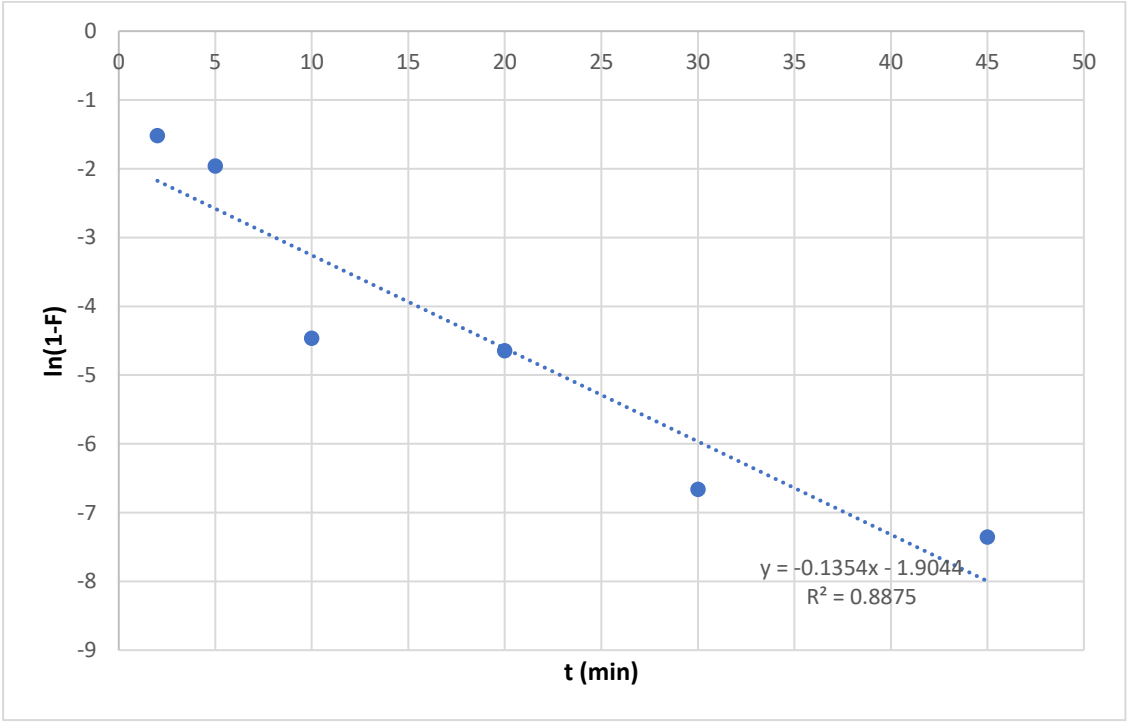


**Fig. 32 The LFD investigation of OXY sorption onto 10%$MoO_3$@$MgAl_2O_4$ composite.**

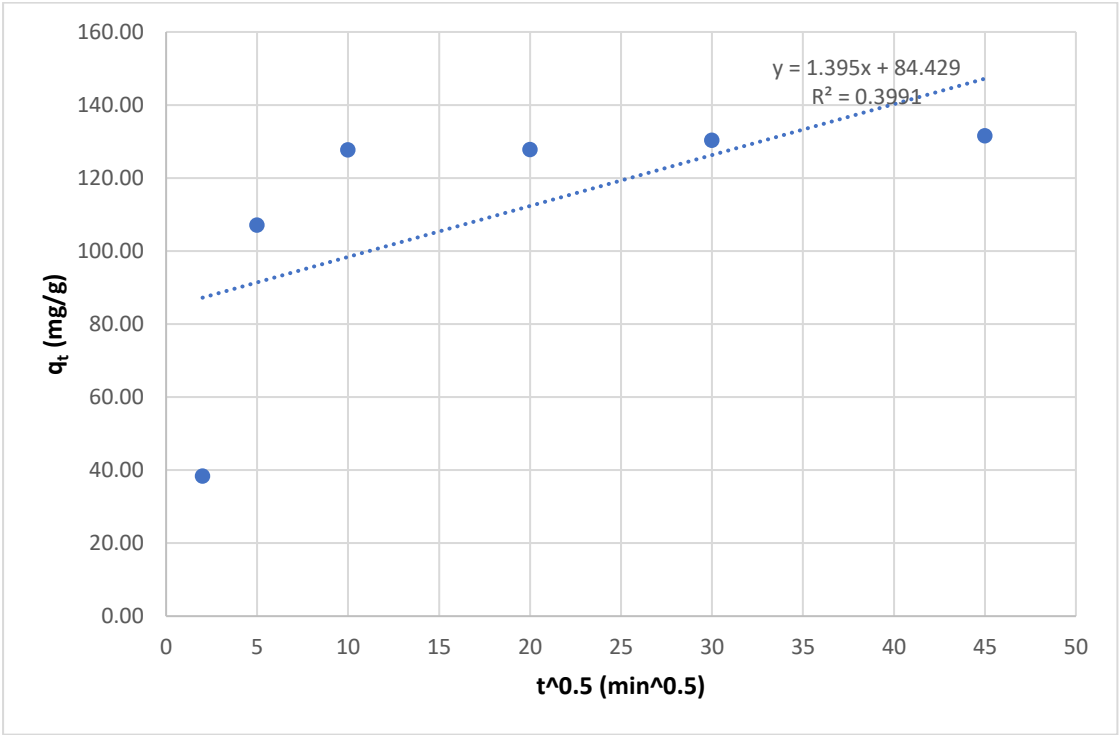


**Fig. 33 The IPD investigation of CIP sorption onto $MgAl_2O_4$ composite.**

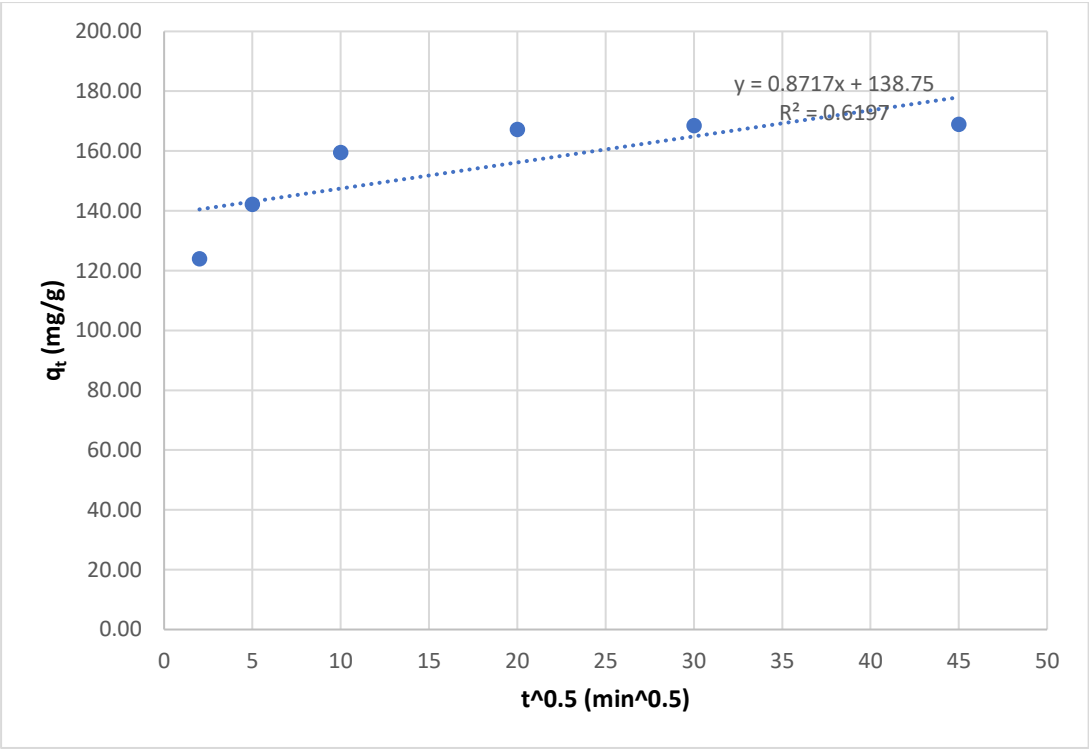


**Fig. 34 The IPD investigation of CIP sorption onto 2.5%$MoO_3$@$MgAl_2O_4$ composite.**

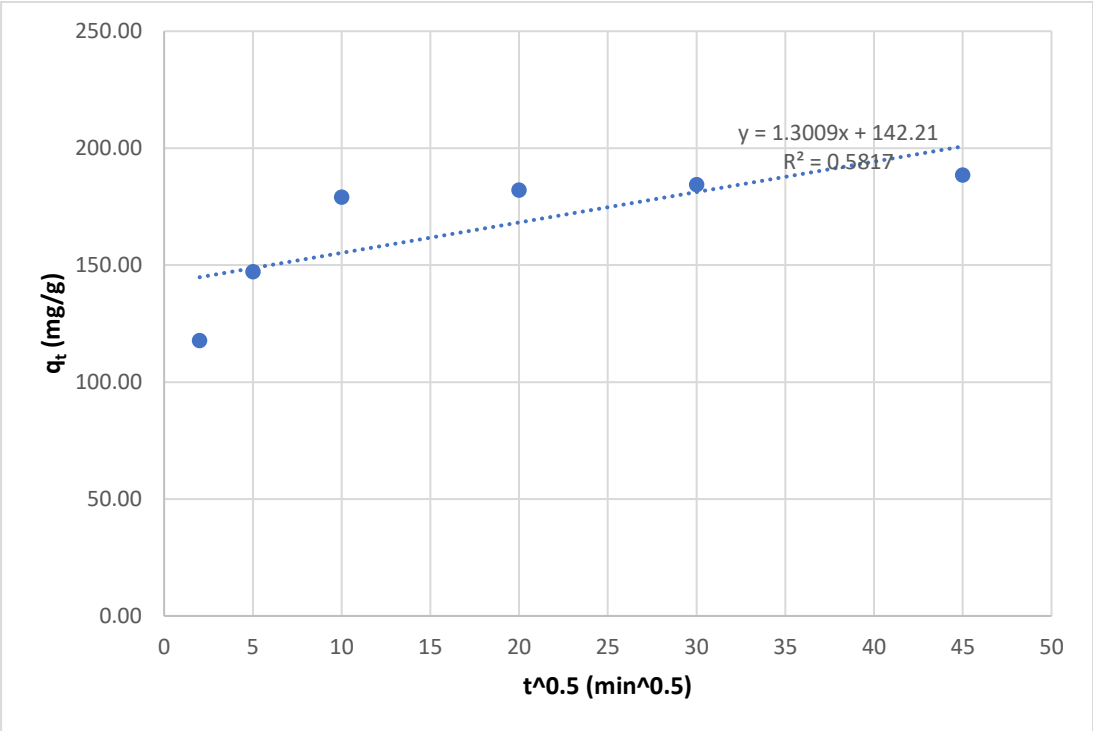


**Fig. 35 The IPD investigation of CIP sorption onto 5%$MoO_3$@$MgAl_2O_4$ composite.**

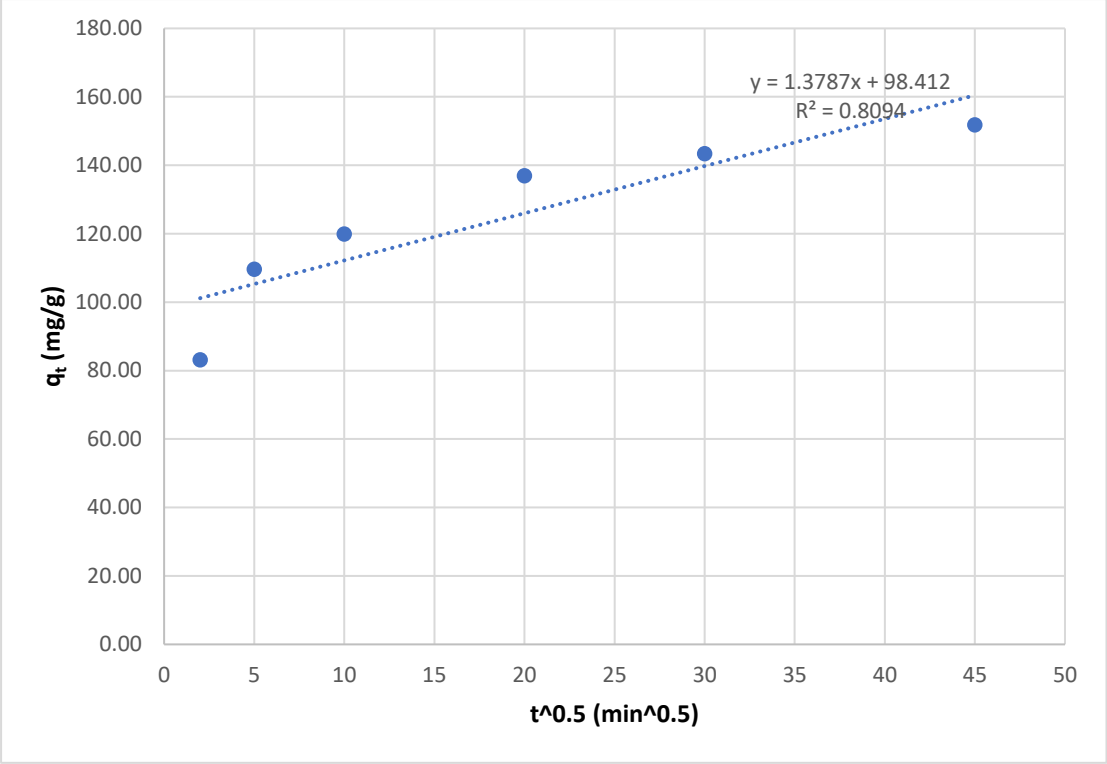


**Fig. 36 The IPD investigation of CIP sorption onto 10%$MoO_3$@$MgAl_2O_4$ composite.**

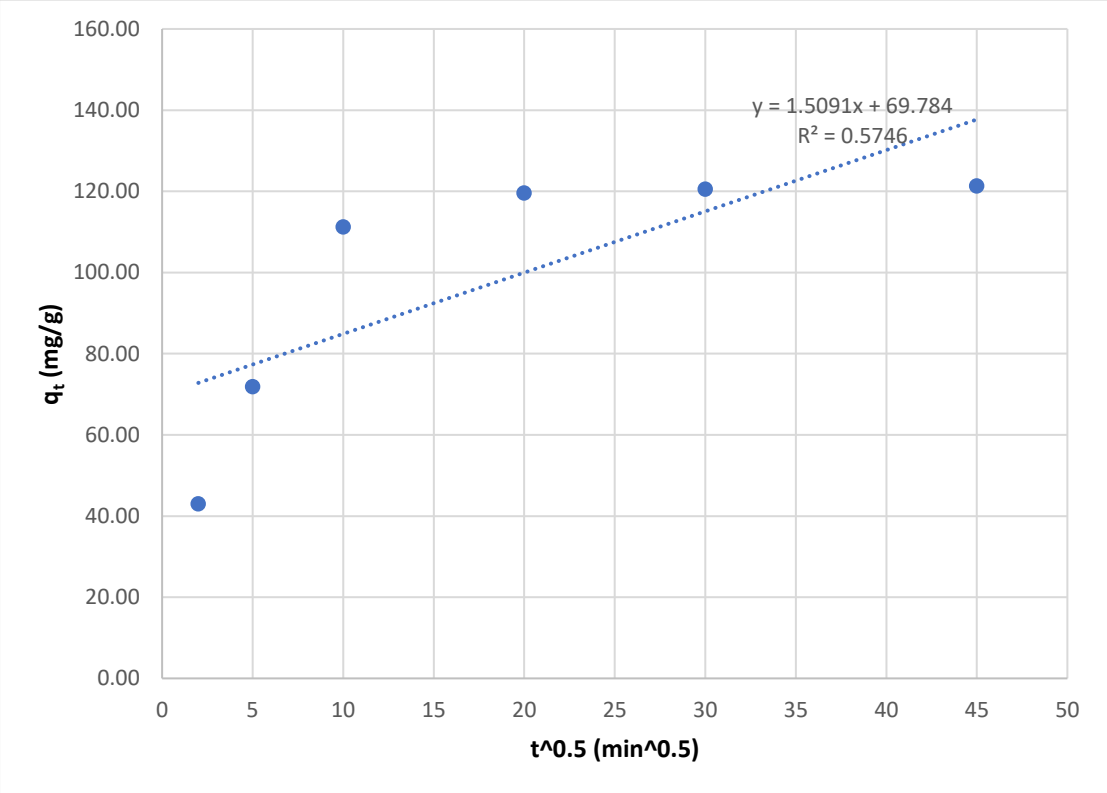


**Fig. 37 The IPD investigation of OXY sorption onto $MgAl_2O_4$ composite**

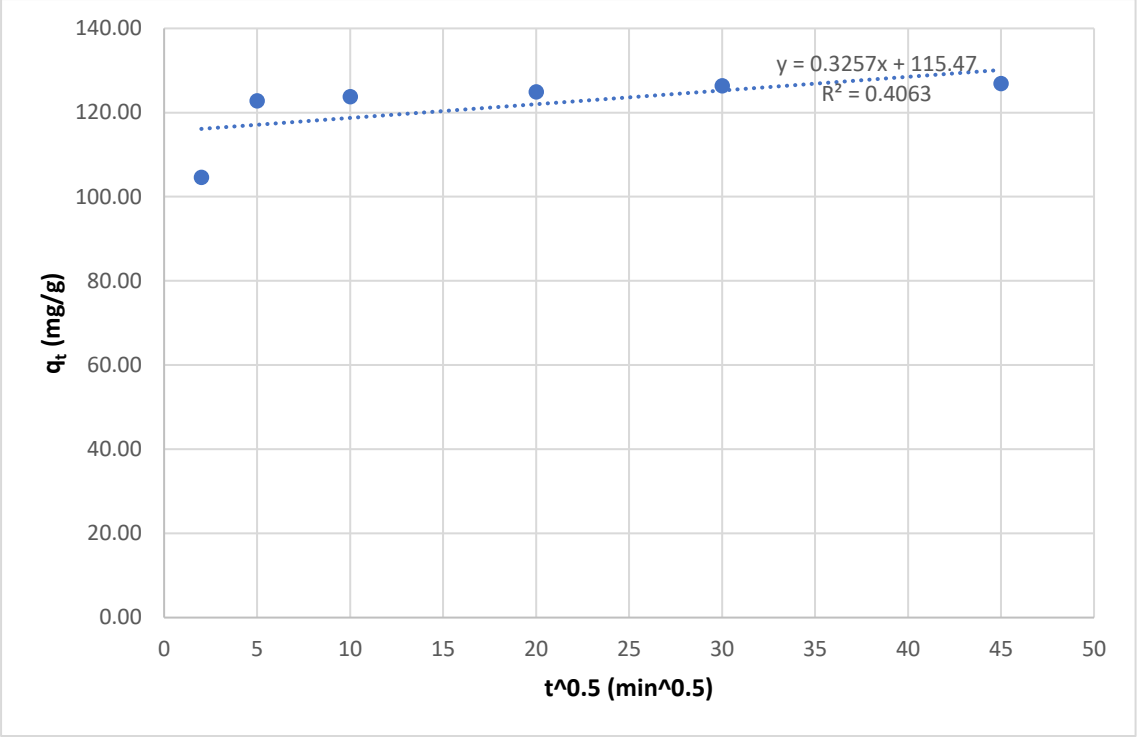


**Fig. 38 The IPD investigation of OXY sorption onto 2.5%$MoO_3$@$MgAl_2O_4$ composite.**

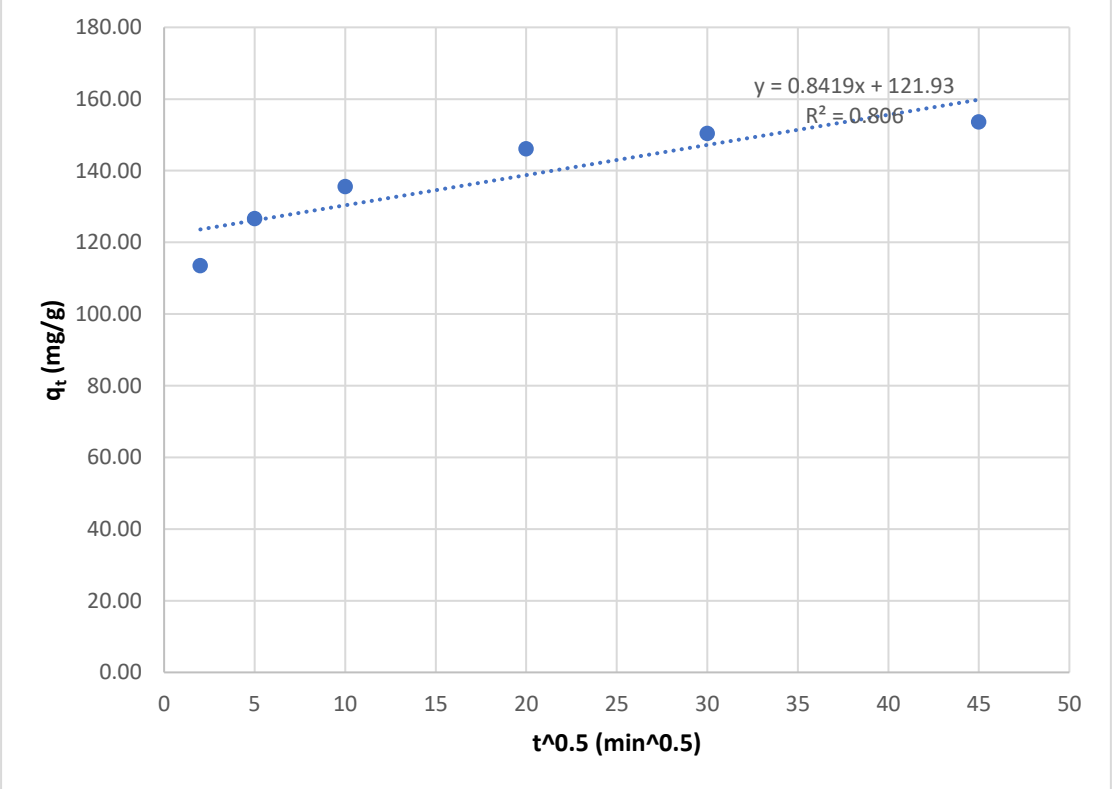


**Fig. 39 The IPD investigation of OXY sorption onto 5%$MoO_3$@$MgAl_2O_4$ composite.**

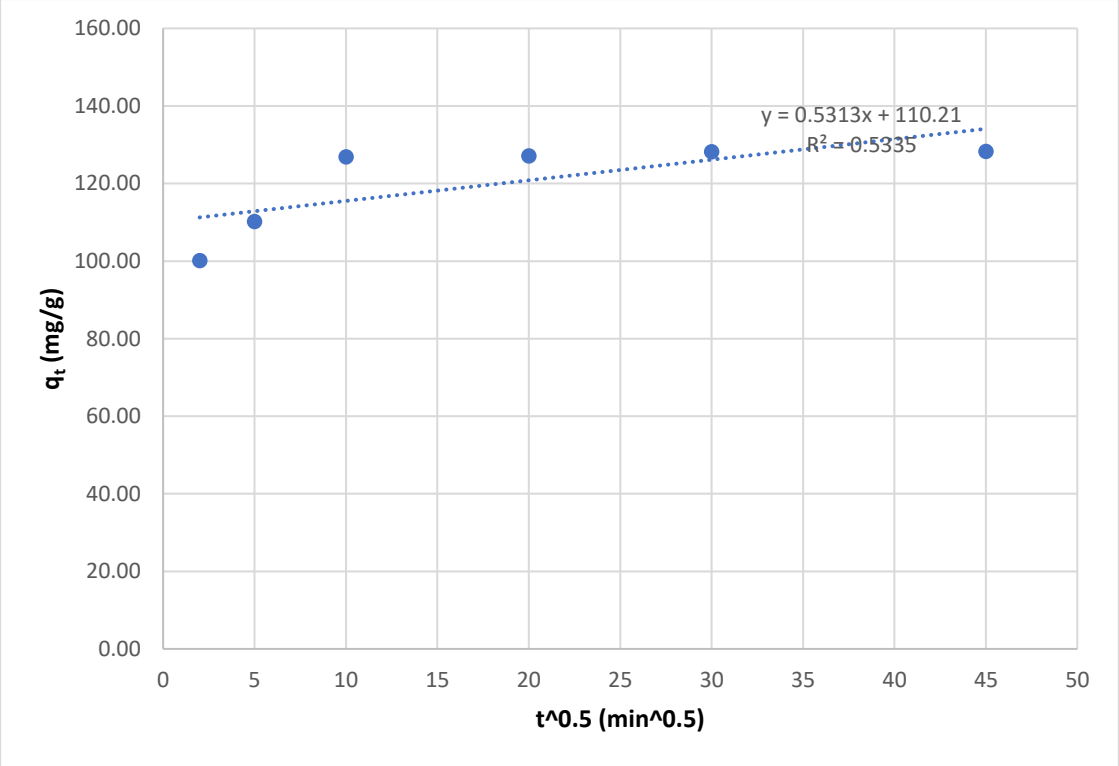


**Fig. 40 The IPD investigation of OXY sorption onto 10%$MoO_3$@$MgAl_2O_4$ composite.**

**Table 3 The adsorption rate control results of CIP removal by $MgAl_2O_4$, 2.5%$MoO_3$@$MgAl_2O_4$, 5%$MoO_3$@$MgAl_2O_4$, and 10%$MoO_3$@$MgAl_2O_4$.**

| Sorbent | *LFDM* | | *IPDM* | |
|---|---|---|---|---|
| | $K_{LF}$ ($min^{-1}$) | $R^2$ | $K_{IP}$ (mg $g^{-1}$ $min^{0.5}$) | $R^2$ |
| AlMgO4 | 0.053581 | 0.637 | 13.499 | 0.5535 |
| 2.5%$MoO_3$@$AlMgO_4$ | 0.118085 | 0.947 | 8.044 | 0.7815 |
| 5%$MoO_3$@$AlMgO_4$ | 0.07215 | 0.878 | 12.053 | 0.7396 |
| 10%$MoO_3$@$AlMgO_4$ | 0.06173 | 0.988 | 12.096 | 0.9228 |

**Table 4 The adsorption rate control results of OXY removal by $MgAl_2O_4$, 2.5%$MoO_3$@$MgAl_2O_4$, 5%$MoO_3$@$MgAl_2O_4$, and 10%$MoO_3$@$MgAl_2O_4$.**

| Sorbent | *LFDM* | | *IPDM* | |
|---|---|---|---|---|
| | $K_{LF}$ ($min^{-1}$) | $R^2$ | $K_{IP}$ (mg $g^{-1}$ $min^{0.5}$) | $R^2$ |
| AlMgO4 | 0.156 | 0.974 | 14.058 | 0.7384 |
| 2.5%$MoO_3$@$AlMgO_4$ | 0.051 | 0.743 | 3.106 | 0.5473 |
| 5%$MoO_3$@$AlMgO_4$ | 0.111 | 0.967 | 7.416 | 0.9263 |
| 10%$MoO_3$@$AlMgO_4$ | 0.135 | 0.888 | 4.985 | 0.6955 |

### 3.4. Conclusion

This study used a one-put fast method to prepare $MgAl_2O_4$, 2.5%$MoO_3$@$MgAl_2O_4$, 5%$MoO_3$@$MgAl_2O_4$, and 10%$MoO_3$@$MgAl_2O_4$ composites. The synthesized composites were studied for removing CIP and OXY from the water via adsorption. The $MgAl_2O_4$, 2.5%$MoO_3$@$MgAl_2O_4$, 5%$MoO_3$@$MgAl_2O_4$, and 10%$MoO_3$@$MgAl_2O_4$ showed $q_t$ values for CIP were 137.0, 169.2, 190.9 and 156.0 mg $g^{-1}$, respectively, while for OXY they showed $q_t$ values of 121.4, 128.3, 153.9 and 128.4 mg $g^{-1}$, respectively. The CIP sorption reached its equilibrium at 60 minutes, while 30 minutes was sufficient for OXY sorption equilibration onto the four sorbents. It is worth mentioning that 90% of the gained CIP and OXY $q_t$ values were acquired within the first 20 and 10 minutes, respectively. The adsorption rate order of CIP and OXY removal by $MgAl_2O_4$, 2.5%$MoO_3$@$MgAl_2O_4$, 5%$MoO_3$@$MgAl_2O_4$, and 10%$MoO_3$@$MgAl_2O_4$ was studied via PF and PS kinetic models. The rate-order outputs of CIP removal illustrated that its sorption by the four sorbents fitted PS except for 10%$MoO_3$@$MgAl_2O_4$, which followed the PF. Additionally, the OXY rate investigation output revealed the agreement of OXY sorption onto the four sorbents to the PS, except for the 2.5%$MoO_3$@$MgAl_2O_4$, which fitted the PF. Furthermore, the rate-control mechanism of CIP and OXY removals by $MgAl_2O_4$, 2.5%$MoO_3$@$MgAl_2O_4$, 5%$MoO_3$@$MgAl_2O_4$, and 10%$MoO_3$@$MgAl_2O_4$ was studied via the IPD and LFD model. Their outputs unraveled that LFD controlled CIP and OXY removals by the four sorbents.

# References


1. Hasan, S.J.R.J.R.S., *A review on nanoparticles: their synthesis and types.* 2015. **2277**: p. 2502.
2. Biswas, P., C.-Y.J.J.o.t.a. Wu, and w.m. association, *Nanoparticles and the environment.* 2005. **55**(6): p. 708-746.
3. Tissue, B. and H.J.J.o.S.S.C. Yuan, *Structure, particle size, and annealing of gas phase-condensed Eu3+: Y2O3 nanophosphors.* 2003. **171**(1-2): p. 12-18.
4. Hasany, S., et al., *Systematic review of the preparation techniques of iron oxide magnetic nanoparticles.* 2012. **2**(6): p. 148-158.
5. Arole, V. and S.J.J.M.S. Munde, *Fabrication of nanomaterials by top-down and bottom-up approaches-an overview.* 2014. **1**: p. 89-93.
6. Houshiar, M., et al., *Synthesis of cobalt ferrite (CoFe2O4) nanoparticles using combustion, coprecipitation, and precipitation methods: A comparison study of size, structural, and magnetic properties.* 2014. **371**: p. 43-48.
7. Ma, J., et al., *Preparation of cobalt ferrite nanoparticles via a novel solvothermal approach using divalent iron salt as precursors.* 2013. **48**(2): p. 214-217.
8. Minemoto, T., et al., *Preparation of Zn1− xMgxO films by radio frequency magnetron sputtering.* 2000. **372**(1-2): p. 173-176.
9. Ostwald, W.J.P.C., *On the Formation of Liesegang Rings.* 1897. **27**: p. 365.
10. Rayleigh, L.J.T.L., Edinburgh,, D.P. Magazine, and J.o. Science, *LXXVIII. Periodic precipitates.* 1919. **38**(228): p. 738-740.
11. Alexander, J., *Colloid Chemistry, Theoretical and Applied: Theory and methods*. Vol. 1. 1926: Chemical Catalog Company.
12. Stöber, W., et al., *Controlled growth of monodisperse silica spheres in the micron size range.* 1968. **26**(1): p. 62-69.
13. Tan, C., et al., *Production of monodisperse colloidal silica spheres: Effect of temperature.* 1987. **118**(1): p. 290-293.
14. Tadic, M., et al., *Magnetic properties of novel superparamagnetic iron oxide nanoclusters and their peculiarity under annealing treatment.* 2014. **322**: p. 255-264.
15. Sun, C., et al., *Versatile application of a modern scanning electron microscope for materials characterization.* 2020. **55**(28): p. 13824-13835.
16. Manahan, S., *Environmental chemistry*. 2017: CRC press.
17. Ruhoy, I.S. and C.G.J.E.i. Daughton, *Beyond the medicine cabinet: an analysis of where and why medications accumulate.* 2008. **34**(8): p. 1157-1169.
18. Zhao, Y. and X. Xiao, *Environmental Antibiotics: Exposure Monitoring and Health Endpoints*, in *Emerging Chemicals and Human Health*. 2019, Springer. p. 165-178.
19. Gupta, R., B. Sati, and A. Gupta, *Treatment and recycling of wastewater from pharmaceutical industry*, in *Advances in Biological Treatment of Industrial Waste Water and their Recycling for a Sustainable Future*. 2019, Springer. p. 267-302.
20. MISHRA, R., et al., *INVESTIGATION OVER WATER QUALITY OF RIVERS GANGA AND YAMUNA DURING KUMBH-2019-A CASE STUDY AT PRAYAGRAJ (ALLAHABAD), UTTAR PRADESH, INDIA.*
21. Yihdego, Z.J.B.R.P.i.I.W.L., *The fairness 'dilemma'in sharing the Nile waters: what lessons from the grand Ethiopian renaissance dam for international law?* 2017. **2**(2): p. 1-80.
22. Verma, J., et al., *Marine pollution, sources, effect and management.* Three Major Dimensions of Life: Environment, Agriculture and Health. Prayagraj, India: Society of Biological Sciences and Rural Development, 2020: p. 270-276.
23. Sjerps, R.M., et al., *Occurrence of pesticides in Dutch drinking water sources.* 2019. **235**: p. 510-518.
24. Pan, Z., et al., *Environmental implications of microplastic pollution in the Northwestern Pacific Ocean.* 2019. **146**: p. 215-224.

25. Yadav, K.K., et al., *Fluoride contamination, health problems and remediation methods in Asian groundwater: A comprehensive review.* 2019. **182**: p. 109362.
26. Lee, H., et al., *Emergence and spread of cephalosporin-resistant Neisseria gonorrhoeae with mosaic penA alleles, South Korea, 2012–2017.* 2019. **25**(3): p. 416.
27. Gleick, P.H. and M.J.P.o.t.N.A.o.S. Palaniappan, *Peak water limits to freshwater withdrawal and use.* 2010. **107**(25): p. 11155-11162.
28. Stumm-Zollinger, E. and G.M. Fair, *Biodegradation of steroid hormones.* Journal (Water Pollution Control Federation), 1965: p. 1506-1510.
29. Daughton, C.G. and T.A. Ternes, *Pharmaceuticals and personal care products in the environment: agents of subtle change?* Environmental health perspectives, 1999. **107**(suppl 6): p. 907-938.
30. Wu, C., et al., *Water pollution and human health in China.* 1999. **107**(4): p. 251-256.
31. Chander, V., et al., *Pharmaceutical compounds in drinking water.* 2016. **6**(1): p. 5774.
32. Kairigo, P., et al., *Contamination of surface water and river sediments by antibiotic and antiretroviral drug cocktails in low and middle-income countries: occurrence, risk and mitigation strategies.* 2020. **12**(5): p. 1376.
33. Ibrahim, T.G., et al., *A Thorough Examination of the Solution Conditions and the Use of Carbon Nanoparticles Made from Commercial Mesquite Charcoal as a Successful Sorbent for Water Remediation.* Nanomaterials, 2023. **13**(9): p. 1485.
34. Almufarij, R.S., et al., *Sweep-Out of Tigecycline, Chlortetracycline, Oxytetracycline, and Doxycycline from Water by Carbon Nanoparticles Derived from Tissue Waste.* Nanomaterials, 2022. **12**(20): p. 3617.
35. Topare, N.S. and S.A. Bokil, *Adsorption of textile industry effluent in a fixed bed column using activated carbon prepared from agro-waste materials.* Materials Today: Proceedings, 2021.
36. Yurtsever, A., et al., *Self-forming dynamic membrane bioreactor for textile industry wastewater treatment.* Science of The Total Environment, 2021. **751**: p. 141572.
37. Feng, Q., et al., *Flocculation performance of papermaking sludge-based flocculants in different dye wastewater treatment: Comparison with commercial lignin and coagulants.* Chemosphere, 2021. **262**: p. 128416.
38. Othman, M.H.D., et al., *Advanced Membrane Technology for Textile Wastewater Treatment*, in *Membrane Technology Enhancement for Environmental Protection and Sustainable Industrial Growth*. 2021, Springer. p. 91-108.
39. Chowdhury, M.F., et al., *Current treatment technologies and mechanisms for removal of indigo carmine dyes from wastewater: A review.* Journal of Molecular Liquids, 2020: p. 114061.
40. Harrache, Z., et al., *Thermodynamic and kinetics studies on adsorption of Indigo Carmine from aqueous solution by activated carbon.* Microchemical Journal, 2019. **144**: p. 180-189.
41. Oberoi, A.S., et al., *Insights into the fate and removal of antibiotics in engineered biological treatment systems: a critical review.* Environmental science & technology, 2019. **53**(13): p. 7234-7264.
42. Jones, O.A., J.N. Lester, and N.J.T.i.B. Voulvoulis, *Pharmaceuticals: a threat to drinking water?* 2005. **23**(4): p. 163-167.
43. Hussin, F., M.K. Aroua, and M.A.J.E. Kassim, *Transforming Plastic Waste into Porous Carbon for Capturing Carbon Dioxide: A Review.* 2021. **14**(24): p. 8421.